

Effects of Roll Vortices on the Evolution of Hurricane Harvey during Landfall

XIN LI,^a ZHAOXIA PU,^a AND ZHIQIU GAO^b

^a *Department of Atmospheric Sciences, University of Utah, Salt Lake City, Utah*

^b *Institute of Atmospheric Physics, Chinese Academy of Sciences, Beijing, China*

(Manuscript received 4 September 2020, in final form 24 March 2021)

ABSTRACT: Horizontal boundary layer roll vortices are a series of large-scale turbulent eddies that prevail in a hurricane's boundary layer. In this paper, a one-way nested sub-kilometer-scale large-eddy simulation (LES) based on the Weather Research and Forecasting (WRF) Model was used to examine the impact of roll vortices on the evolution of Hurricane Harvey around its landfall from 0000 UTC 25 August to 1800 UTC 27 August 2017. The simulation results imply that the turbulence in the LES can be attributed mainly to roll vortices. With the representation of roll vortices, the LES provided a better simulation of hurricane wind vertical structure and precipitation. In contrast, the mesoscale simulation with the YSU PBL scheme overestimated the precipitation for the hurricane over the ocean. Further analysis indicates that the roll vortices introduced a positive vertical flux and thinner inflow layer, whereas a negative flux maintained the maximum tangential wind at around 400 m above ground. During hurricane landfall, the weak negative flux maintained the higher wind in the LES. The overestimated low-level vertical flux in the mesoscale simulation with the YSU scheme led to overestimated hurricane intensity over the ocean and accelerated the decay of the hurricane during landfall. Rainfall analysis reveals that the roll vortices led to a weak updraft and insufficient water vapor supply in the LES. For the simulation with the YSU scheme, the strong updraft combined with surplus water vapor eventually led to unrealistic heavy rainfall for the hurricane over the ocean.

KEYWORDS: Hurricanes; Boundary layer; Large eddy simulations

1. Introduction


Horizontal boundary layer roll vortices are a series of large-scale turbulent eddies that align along the mean wind direction (Etling and Brown 1993). They can be found in a neutral or weakly unstable atmospheric boundary layer (Mourad and Walter 1996; Weckwerth et al. 1997; Young et al. 2002) and in a hurricane boundary layer (Wurman and Winslow 1998; Katsaros et al. 2000, 2002; Lorusso et al. 2008; Ellis and Businger 2010; Huang et al. 2018). Similar to those in an Ekman flow, the roll vortices in a hurricane boundary layer are generated mainly by inflection point instability (Lilly 1966; Brown 1980), which is caused by the sharp reduction of inflow vertically (i.e., vertical wind shear; Foster 2005; Gao and Ginis 2014). Morrison et al. (2005) found that roll vortices can extend from 200 to 800 m above the ground in the hurricane boundary layer. These large-scale eddies can generate strong fluxes and govern the energy, momentum, and composition exchange in the hurricane boundary layer (Morrison et al. 2005; Zhang et al. 2008).

Due to the lack of observations, numerical simulations have been an effective tool to study roll vortices. Large-eddy simulation (LES) is particularly useful in this regard, as it resolves the most important scale of flow and approximates other scales of turbulence (Wu et al. 2019). Previous studies have verified the capacity of LES to capture large-scale rolls in the

hurricane boundary layer (Nakanishi and Niino 2012; Wang and Jiang 2017).

To understand the effect of roll vortices in hurricanes, Gao and Ginis (2014, 2016, 2018) and Gao et al. (2017) used ideal large-eddy models to simulate roll vortices. From a series of numerical simulations, they found that roll vortices can lead to countergradient fluxes and can change the wind structure in a hurricane. Since a change in wind structure can lead to different surface winds, ideal simulation results indicated that roll vortices in a hurricane could influence the degree of damage a hurricane can inflict during its landfall due to their effects on hurricane intensity and structure. Nevertheless, despite great progress with idealized models, the effect of roll vortices has not been confirmed with real hurricane cases because of inadequate high-resolution observations, with particular focus on the structure of roll vortices (Wurman and Winslow 1998; Katsaros et al. 2000, 2002), and numerical simulations with real hurricanes. Limited by computational resources, many previous studies of real cases have simulated the hurricane boundary layer during only a short period, with emphasis on the turbulent characteristics of roll vortices (Zhu et al. 2016; Zhu 2008a,b). The evolution of roll vortices and their interaction with the hurricane boundary layer and associated weather phenomena (e.g., precipitation) have not yet been studied in detail. Specifically, the intensity and structure of the gusting winds and rainfall of a landfalling hurricane are important in determining damage after landfall. Thus, there is a need to study the effects of roll vortices on hurricane winds and precipitation during hurricane landfall.

With advances in numerical weather prediction models and mesoscale community models, hurricane simulations and predictions have achieved approximately 1 km horizontal

 Denotes content that is immediately available upon publication as open access.

Corresponding author: Prof. Zhaoxia Pu, zhaoxia.pu@utah.edu

resolution (Kunin et al. 2019; Li et al. 2020). Through high-resolution simulations, the small-scale structure of a hurricane can be captured. However, roll vortices usually have a mean wavelength of about 1.5 km (Morrison et al. 2005), and in some cases less than 1 km. Mesoscale simulations with a horizontal resolution of about 1 km cannot adequately simulate roll vortices in the hurricane boundary layer. Meanwhile, the planet boundary layer (PBL) parameterization scheme used in mesoscale simulations may not be sufficient to simulate the impact of roll vortices on hurricane evolution. The gap between the PBL parameterization scheme and the actual physical processes may lead to larger errors in simulations of hurricanes and limit the development of numerical simulation models. Therefore, to assess the PBL parameterization scheme and verify the impact of roll vortices, in this study a high-resolution LES with a real hurricane was set up and compared to mesoscale simulations. Combining mesoscale simulations and LES in an Advanced Research version of the Weather Research and Forecasting (WRF) Model (Skamarock et al. 2008), we employ the WRF-LES model to simulate Hurricane Harvey (2017) during its landfall. Considering the significant damage caused by Hurricane Harvey, we focus on the simulation and analysis of the effects of the horizontal boundary layer roll vortices on hurricane intensity and rainfall during the simulation period. Simulations with the PBL parameterization scheme and with LES are also compared to assess the deficiencies of the PBL scheme in representing the hurricane boundary layer.

The WRF-LES model setup and turbulence data processing are described in section 2. Verification of simulation results is provided in section 3. Impact analysis of the horizontal boundary layer roll vortices for hurricane wind and precipitation is provided in sections 4 and 5, respectively. A sensitivity study is described in section 6, and a summary and conclusions are presented in section 7.

2. Model and turbulence fields

a. WRF-LES model

This study uses a nested-domain configuration of the WRF Model (version 3.9.1.1) to achieve a high-resolution LES of Hurricane Harvey (2017) around its landfall from 0000 UTC 25 August to 1800 UTC 27 August 2017. As shown in Fig. 1, the first two domains were set up with the Yonsei University PBL scheme (Hong et al. 2006; Hong 2010) to generate large-scale background synoptic and mesoscale flow situations. We used the inner two domains to simulate the hurricane turbulent eddy structure with LES. The horizontal resolution for the four domains was set at 12.5, 2.5, 0.5, and 0.1 km, respectively. They were configured with grid meshes of 150×150 , 251×281 , 951×1131 , and 1401×1401 , respectively. To better simulate the hurricane boundary layer, 71 vertical levels were used, of which 39 levels were below 1500 m, with the lowest model level approximately 3 m. During hurricane landfall, domain 4 was moved with time to simulate the inner core of Hurricane Harvey: domain 4-1 (D4-1 in Fig. 1) was from 0600 to 1800 UTC 25 August 2017; domain 4-2 (D4-2 in Fig. 1) from

1800 UTC 25 August to 1200 UTC 26 August 2017; and domain 4-3 (D4-3 in Fig. 1) from 1200 UTC 26 August to 1800 UTC 27 August 2017. The spinup of the first two domains was from 0000 to 0600 UTC 25 August, and this then drove the two inner domains. To avoid irregularities during the moving domain, we performed another spinup on domain 1 and 2 before moving domain 4. For instance, the spinup of the first two domains was from 1200 to 1800 UTC 25 August, and then the inner two domains were run.

The Yonsei University (YSU) PBL scheme is used in domains 1 and 2. For the LES, the PBL scheme was deactivated in the two inner domains (domains 3 and 4), and subgrid-scale turbulence derived by the TKE 1.5 closure scheme was used. A one-way nested configuration was used for the simulation to prevent interaction between different domains during the integration. The Kain and Fritsch (Kain 2004) deep convection scheme was activated only in domain 1. For other physics parameterizations, the Thompson cloud physics scheme (Thompson et al. 2008), Rapid Radiative Transfer Model (RRTM; Mlawer et al. 1997), Dudhia scheme (Dudhia 1989), Noah land surface scheme (Chen and Dudhia. 2001), and revised MM5 Monin–Obukhov scheme were used for cloud, longwave radiation, shortwave radiation, land surface, and surface parameterizations. The U.S. National Centers for Environmental Prediction (NCEP) Global Forecast System (GFS) final analysis (FNL) $0.25^\circ \times 0.25^\circ$ data were used to initialize the simulation and provide outer boundary conditions.

b. Turbulence fields

For the first two domains, the turbulence flux was generated directly from the YSU scheme (Hong et al. 2006; Hong 2010). For the two inner domains, we applied a horizontal two-dimensional Gaussian filter to the simulation results for smoothing and then produced the turbulence fields by subtracting the smoothed field from the simulation. The Gaussian filter is described as follows:

$$G(x, y) = \frac{1}{2\pi\sigma^2} e^{-(x^2+y^2)/(2\pi\sigma^2)}, \quad (1)$$

where x and y are the grids in the x and y directions. To better compare with the results in domain 2, the bandwidth, which indicates the filter region, was set at 5×5 for domain 3 and 25×25 for domain 4, with a Gaussian function standard deviation σ of 10. Only grids with a distance less than 2.5 km were considered in order to smooth the grid data. For variables such as u , v , w , t , and q , the two-dimensional Gaussian filter was used for smoothing, and then the turbulence field was produced by subtracting the smoothed field.

3. Simulation verifications

a. Track and intensity

Figure 1 shows the hurricane track (Fig. 1a) and 10 m wind speed evolution (Fig. 1b) during the simulation period. We found that the simulated hurricane tracks from the four domains were all close to the analyzed hurricane best track from

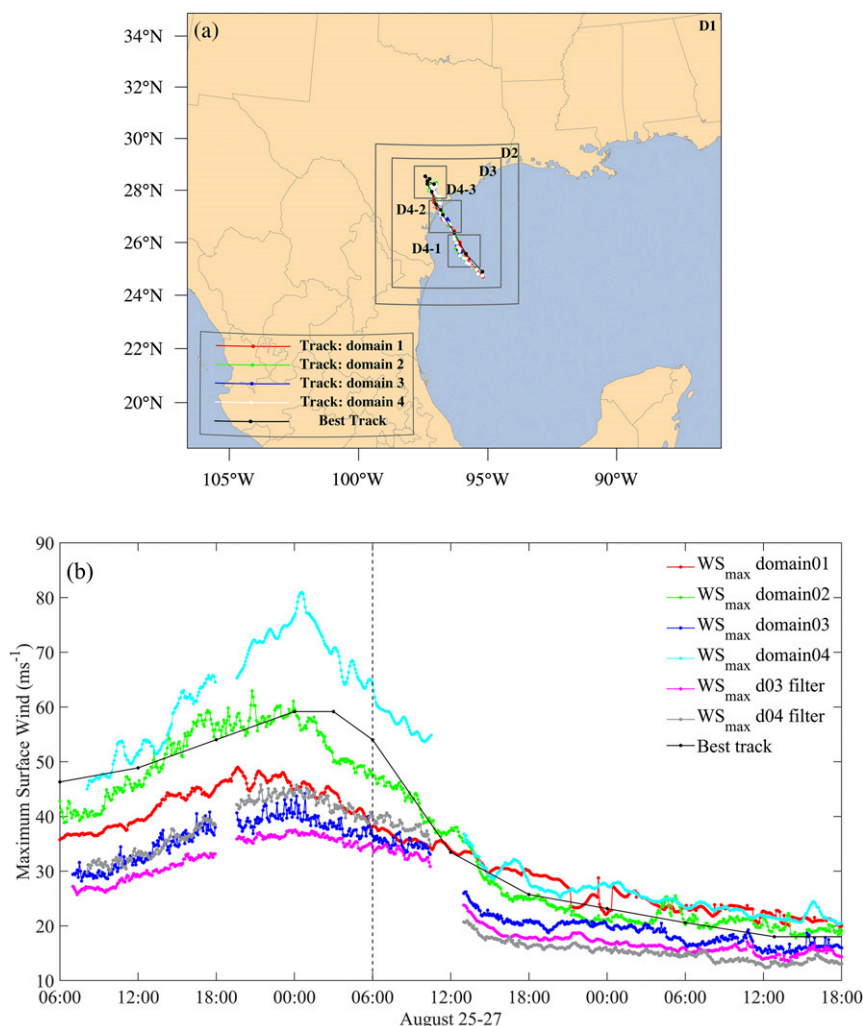


FIG. 1. Illustration of a multiple-scale simulation of Hurricane Harvey during landfall from 0000 UTC 25 Aug to 1800 UTC 27 Aug 2017. (a) The simulated hurricane track compared with the NHC best track. (b) The evolution of maximum 10 m wind during the simulation period from different domains. “ $WS_{\max} \text{ domain}$ ” denotes the maximum 10 m wind at a domain. “ $WS_{\max} \text{ d03filter}$ ” represents the maximum 10 m wind at the domain after applying a filter. Note that if we sample the simulated 10 m winds in domain 4 into the grid spacing of domain 2, the intensity will look the same as that in domain 2 (not shown). The dashed vertical line in (b) denotes landfall time. Because of the spinup in the LES after moving the domain, there is a gap in the 10 m wind speed evolution.

the National Hurricane Center (NHC) report. The simulated hurricane made landfall at 0600 UTC 26 August, a delay of approximately 2–3 h in contrast to the best track, which showed Hurricane Harvey making landfall at 0300 UTC 26 August. Compared to the best track data, the maximum 10 m wind speed was underestimated in domains 1 and 3 and overestimated in domain 4, while it was reasonably simulated in domain 2. After application of the two-dimensional Gaussian filter, the maximum 10 m wind in domains 3 and 4 decreased significantly and was lower than the best track data. The specific instantaneous higher wind speed in domain 4 could be attributed to contribution from strong turbulence, as it can be

eliminated by the two-dimensional Gaussian filter. The high wind in domain 4 was similar to the higher temporal resolution observations from Wurman and Kosiba (2018) and Fernández-Cabán et al. (2019), who also observed surface wind of over 60 m s^{-1} during Hurricane Harvey’s landfall.

b. Wind and precipitation

The simulated wind field and precipitation were compared with the NOAA Hurricane Research Division (HRD) radar wind analysis (https://www.aoml.noaa.gov/hrd/data_sub/radar.html) and the NCEP stage IV precipitation analysis (Lin and Mitchell 2005), respectively. Figure 2 shows the

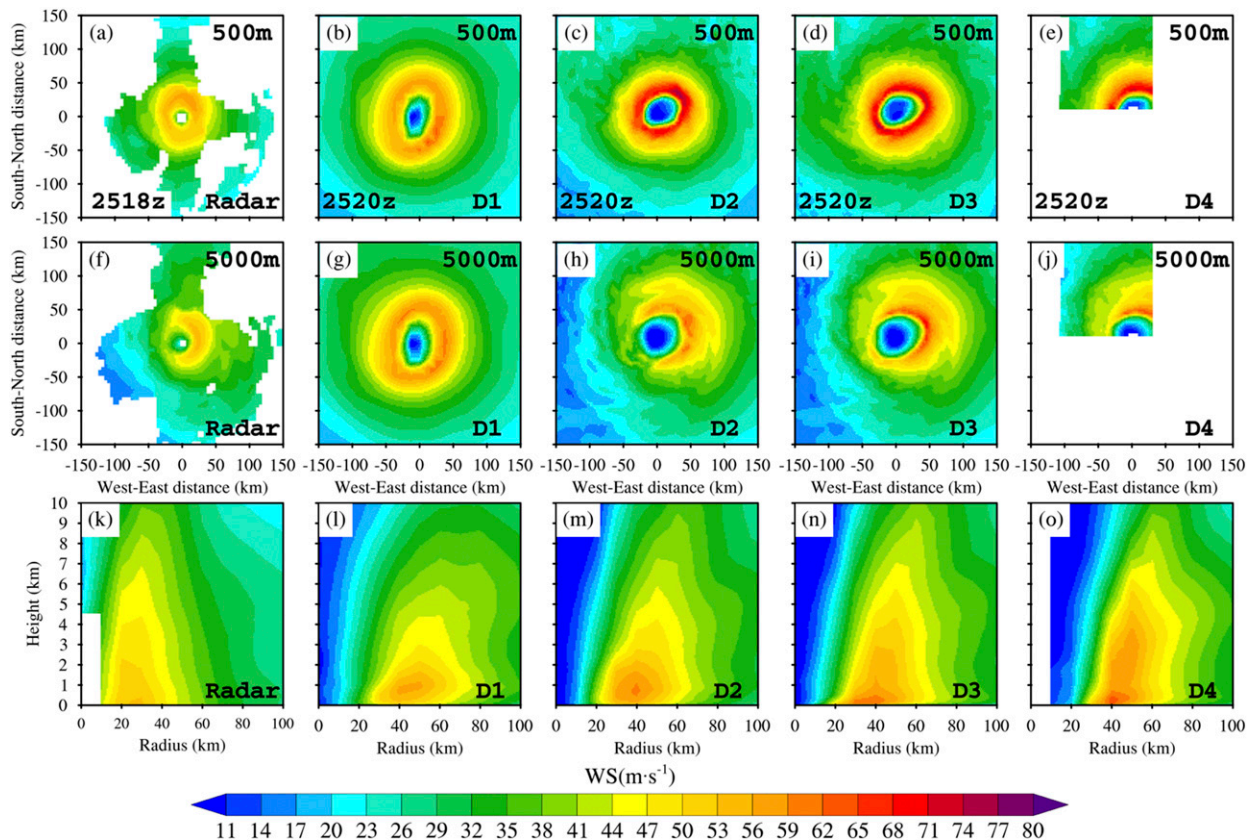


FIG. 2. Comparison of wind speed between Doppler radar wind analysis (from NOAA HRD) at (a),(f),(k) 1800 UTC 25 Aug 2017 and corresponding simulation results (at 2000 UTC 25 Aug 2017 due to delayed landfall time in the simulation) from (b),(g),(l) domain 1, (c),(h),(m) domain 2, (d),(i),(n) domain 3, and (e),(j),(o) domain 4 for a height of (a)–(e) 500 and (f)–(j) 5000 m, and for (k)–(o) azimuthally averaged wind profiles. D1, D2, D3, and D4 denote the simulation results from domains 1, 2, 3, and 4, respectively.

comparison of wind speed between the radar wind analysis (Figs. 2a,f,k) and simulation results from domain 1 (Figs. 2b,g,l), domain 2 (Figs. 2c,h,m), domain 3 (Figs. 2d,i,n), and domain 4 (Figs. 2e,j,o) for a height of 500 m (Figs. 2a–e), 5000 m (Figs. 2f–j), and for azimuthally averaged wind profiles (Figs. 2k–o). The radar data were collected at 1800 UTC 25 August, while the corresponding simulation results were selected at 2000 UTC 25 August because of the 2-h phase (track and intensity) delay for the simulated hurricane. From Fig. 2, we can see that at 500 m the wind speed was higher in domains 2–4, with a maximum speed of over 80 m s^{-1} , and also higher than the observation from Alford et al. (2019), who found over 70 m s^{-1} maximum wind at 500 m. While it was close to the radar data in domain 1, with a maximum wind speed of over 62 m s^{-1} , it was lower than the observation from Alford et al. (2019). At 5000 m, the wind structure in domains 2–4 was close to that in the radar data, with the region of highest wind located in the eastern part of the storm. The wind speed was still slightly higher in domains 2–4, with a maximum of over 62 m s^{-1} . For the vertical structure of wind, the maximum wind speed in domains 3 and 4 was located below 500 m, similar to the radar observations. However, the height of maximum wind speed in domains 1 and 2 was closer to

1000 m. Above the height of maximum wind, in the radar data there was a strong vertical extension trend, with high wind ($45\text{--}47 \text{ m s}^{-1}$) extending up to 6 km. In domains 1 and 2, despite the higher maximum wind than in the radar data, the $45\text{--}47 \text{ m s}^{-1}$ high wind extended up to only 5 km or less. Only in domains 3 and 4 did the $45\text{--}47 \text{ m s}^{-1}$ high wind extend up over 6 km. Therefore, compared to the simulation with the YSU PBL scheme, LES provided better simulations of hurricane wind vertical structure against the radar observations.

Figures 3a–e show the evolution of azimuthally averaged hourly precipitation from the NCEP stage IV data (Fig. 3a), and simulation results in domains 1–4 (Figs. 3b–e). In the stage IV data, the azimuthally averaged hourly precipitation was less than 10 mm h^{-1} before 1600 UTC 25 August, and less than 35 mm h^{-1} before 0100 UTC 26 August. The strongest precipitation occurred from 0200 to 1000 UTC 26 August, with maximum azimuthally averaged hourly precipitation of over 50 mm h^{-1} . However, in domains 1 and 2, the azimuthally averaged precipitation was over 30 mm h^{-1} after 0900 UTC 25 August, and even over 50 mm h^{-1} in domain 2. The strongest precipitation in domain 2 occurred from 0900 UTC 25 August to 0900 UTC 26 August, with maximum azimuthally averaged hourly precipitation of over 50 mm h^{-1} . In domains

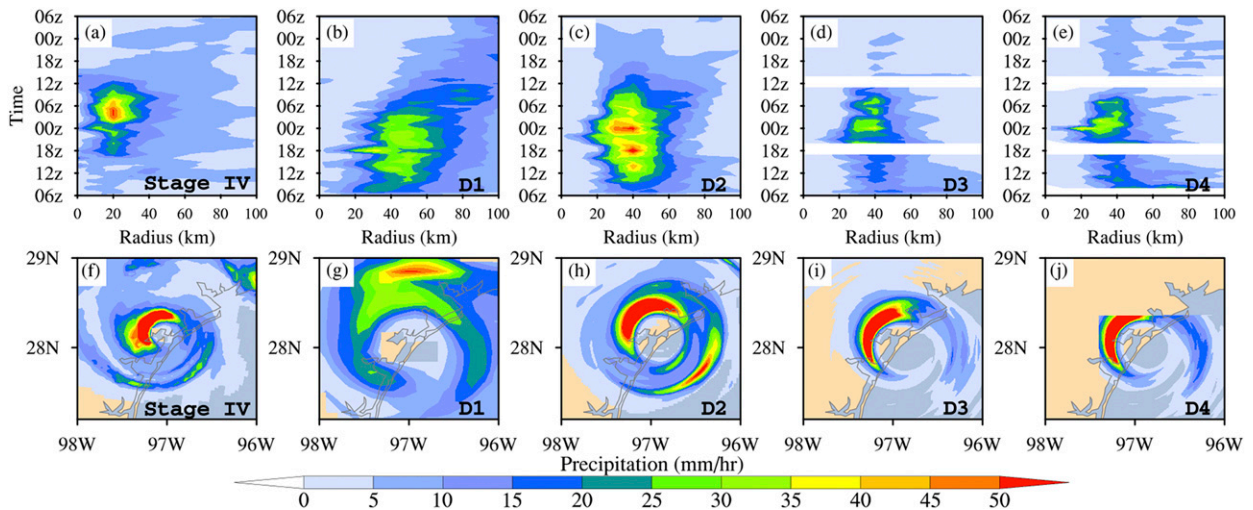


FIG. 3. Evolution of azimuthally averaged hourly precipitation from (a) the NCEP stage IV data, and (b)–(e) simulation results in domains 1–4. (f)–(j) The hourly rainfall from (f) stage IV data and (g)–(j) simulation results in domains 1–4 at 0600 on 26 Aug 2017. The gaps in (d) and (e) are due to restart and spinup in LES during the moving domain. D1, D2, D3, and D4 denote the simulation results from domains 1, 2, 3, and 4, respectively.

3 and 4, the azimuthally averaged precipitation was similar to the stage IV data. The rainfall was less than 25 mm h^{-1} before 1600 UTC 25 August, and the strongest precipitation occurred from 2100 UTC 25 August to 0900 UTC 26 August, with maximum azimuthally averaged hourly precipitation of over 40 mm h^{-1} . Considering that the simulated hurricane had a delay of up to 3 h against the best track, the early overestimated precipitation cannot be attributed to the slowing of the hurricane. The simulations in domains 1 and 2 overestimated the precipitation over the ocean compared to the stage IV dataset. The LESs in domains 3 and 4 reduced this overestimated precipitation for the hurricane over the ocean and were closer to the stage IV data. Figures 3f–j show the hourly precipitation from stage IV (Fig. 3f) and domains 1–4 (Figs. 3g–j) at 0600 UTC 26 August. The overestimated precipitation is evident in domain 2, especially from the southeast to the storm center with over 50 mm h^{-1} . In domains 3 and 4, the northwest rainband is thinner and closer to the stage IV data. Comparing the rainband modification of LES over the ocean and inland, the change is more significant over the ocean, implying that the differences between the YSU scheme and LES results are greater over the ocean but relatively smaller inland. This finding could be a reference for improving simulations with the YSU scheme.

c. Roll vortices

To verify the existence of horizontal boundary layer roll vortices in the LESs, Fig. 4 shows the 10 m wind speed in domains 1 to 4 (Figs. 4a–d) and a cross section (Fig. 4e) in domain 4 (blue line in Fig. 4d) for the vertical component of turbulence vorticity at 1700 UTC 25 August. There were strong perturbations in the 10 m wind in domains 3 and 4, and they tended to be larger in scale in domain 3 than in domain 4. Because of this perturbation in domain 4, there was a rapid wind gradient, with speed varying from 28 to 44 m s^{-1} within a short distance. This

strong perturbation in domain 4 could explain the significant reduction of wind speed after application of the Gaussian filter in Fig. 1b. The cross section of the vertical component of turbulence vorticity shows that there was coupled upward and downward turbulence motion along the cross section, especially in the high wind region (within a radius of 30 to 40 km from the storm center). This coupled upward and downward motion extended from 20 m up to 1500 m, but usually from 20 m up to only 500 m in the low wind region (within a radius greater than 40 km). Also, this coupled turbulence motion in the simulation results shows a similar structure to the observed roll vortices in Morrison et al. (2005), as they both display coupled upward and downward motion along the cross section. Furthermore, Fig. 4f shows the horizontal distribution of this kind of roll at 50 m. The upward and downward turbulence motion is shaded red and blue, respectively. The rolls continuously align along the wind direction, consistent with the findings of Morrison et al. (2005). This coupled upward and downward turbulence motions is associated with the LES perturbations and can be attributed to the development of roll vortices.

Previous studies (Lilly 1966; LeMone 1973; Foster 2005) found that vertical turbulence is generated first by inflection instability and then extends downstream in the mean wind before finally forming roll vortices. Thus, roll vortices are caused by inflection point instability (Lilly 1966; Brown 1980) due to the vertically reduced inflow of wind (wind shear). The sharp reduction of inflow leads to unstable dynamic conditions and, consequently, to the roll vortices in a hurricane boundary layer. To examine whether the perturbations in domain 4 were related to the existence of roll vortices, we first distinguished the contributions of thermal bubbles (buoyancy) and roll vortices (wind shear) to the perturbations in domain 4. The azimuthally averaged buoyancy and wind shear terms in the TKE budget as well as their standard derivations (shaded

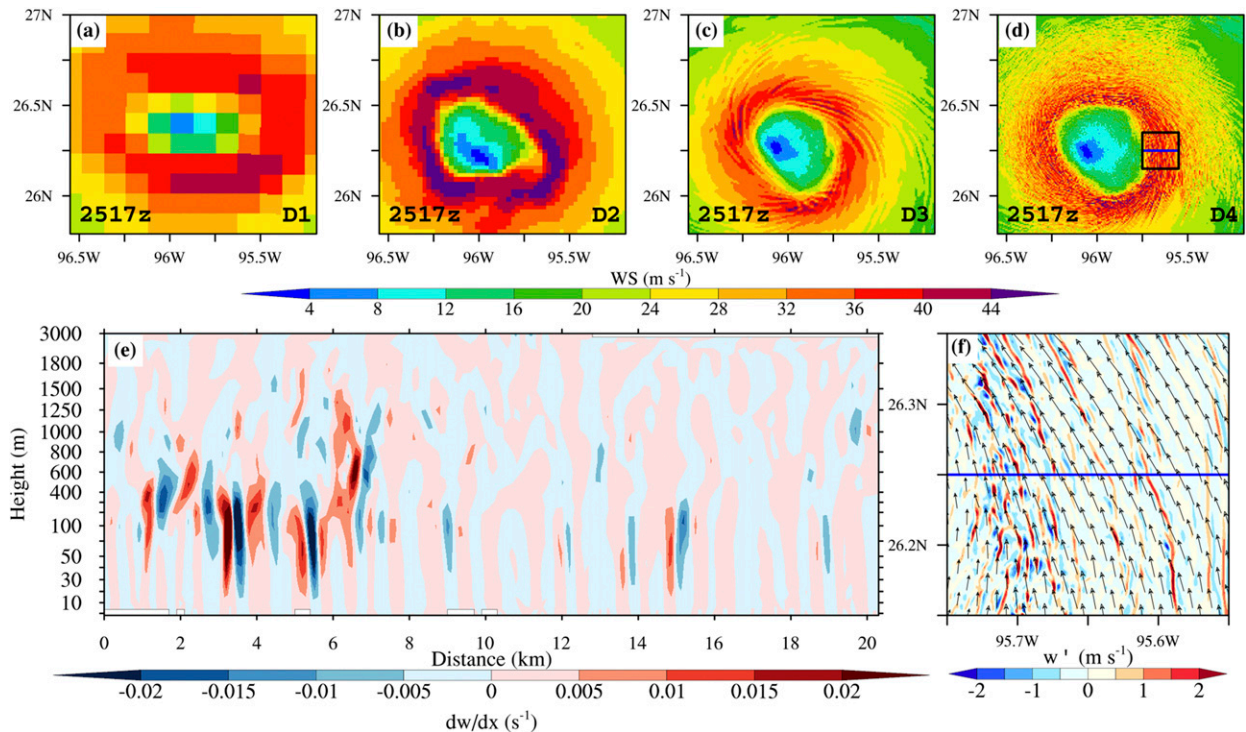


FIG. 4. The 10 m wind from (a) domain 1, (b) domain 2, (c) domain 3, and (d) domain 4 at 1700 UTC 25 Aug 2017. (e) The cross section in domain 4 for the vertical component of turbulence vorticity. The cross section is shown as the blue line in (d) and (f). (f) The horizontal distribution of the turbulence and wind vectors at the height of 50 m in the black box shown in (d). D1, D2, D3, and D4 denote the simulation results from domains 1, 2, 3, and 4, respectively.

contour) were analyzed (Fig. 5) for the hurricane before (Figs. 5a–c) and during (Figs. 5d–f) landfall and inland (Figs. 5g–i). Before landfall, below 200 m, the azimuthally averaged wind shear contributions (to TKE) gradually increased with time from 1200 to 2200 UTC 25 August. As the underlying surface was ocean before landfall, this increased TKE should be related to enhanced roll vortices. The stronger vertical components of roll vortices enhanced the vertical mixing of momentum and increased the TKE. Above 200 m, the azimuthally averaged wind shear contributions gradually increased as well, but with magnitudes significantly smaller than those below 200 m. Meanwhile, the azimuthally averaged buoyancy contributions were very weak and almost negligible compared to the wind shear contributions. During landfall, below 200 m, the azimuthally averaged wind shear contributions continued to increase at 0100 and 0500 UTC and then at 0900 UTC 26 August. Above 200 m, the azimuthally averaged wind shear contributions gradually decreased with time. The azimuthally averaged buoyancy contributions were also weak at all times. For the hurricane inland, the azimuthally averaged wind shear contributions significantly decreased below 200 m and nearly vanished above 200 m. The azimuthally averaged buoyancy contributions were even weaker and disappeared at all levels.

Overall, results from Fig. 5 show that during the whole simulation period, turbulence can be attributed mainly to wind shear, implying the existence of roll vortices. Therefore,

turbulent eddies by roll vortices controlled the turbulence in the LESs.

4. The effect of roll vortices on momentum fluxes and wind structure

From the above analysis, we found roll vortices in the hurricane boundary layer with the LESs. In this section we investigate the effect of these roll vortices on the hurricane's wind structure.

a. Tangential wind

Figure 6 shows the azimuthally averaged tangential wind from all model domains for the hurricane over the ocean at 2200 UTC 25 August (Figs. 6a–d), during landfall at 0500 UTC 26 August (Figs. 6e–h), and inland at 1900 UTC 26 August (Figs. 6i–l). Before landfall, the height of maximum wind was about 1000 m in domains 1 and 2 and about 400 m in domains 3 and 4. Even with the lower height of maximum wind in domains 3 and 4, the maximum wind still extended up to a height of 2000 m. Near the surface, the maximum azimuthally averaged tangential wind reached 30 m s^{-1} within a radius of 30–40 km from the storm center in domains 1 and 2, while it was less than 25 m s^{-1} in domains 3 and 4. During landfall, the height of maximum wind was about 1000 m in domains 1 and 2 and about 400 m in domains 3 and 4. Similarly, the high wind (wind speed greater than 60 m s^{-1}) reached up to 1500 m in

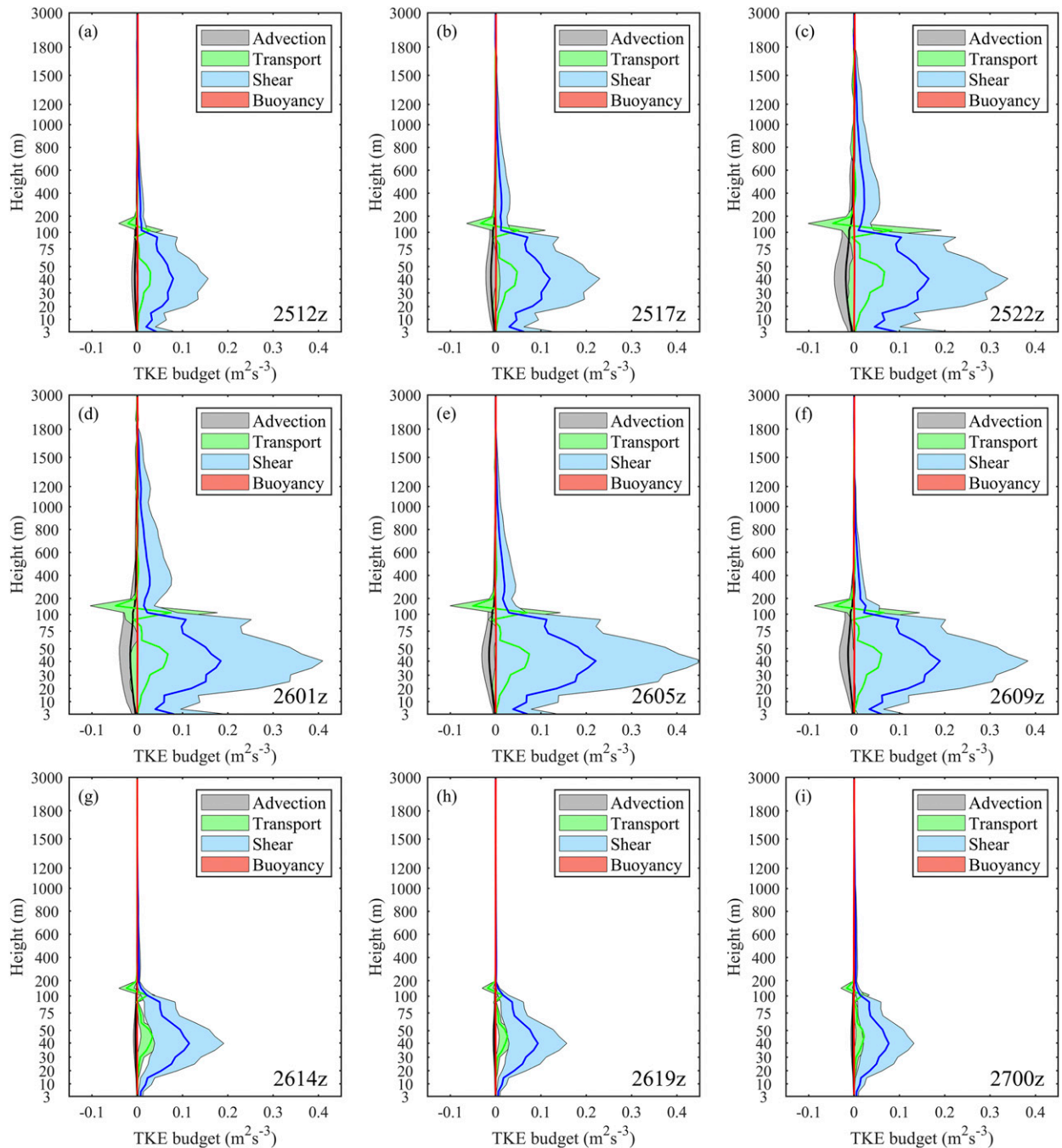


FIG. 5. Azimuthally averaged TKE budget in domain 4 before hurricane landfall at (a) 1200, (b) 1700, and (c) 2200 UTC 25 Aug 2017; during landfall at (d) 0100, (e) 0500, and (f) 0900 UTC 26 Aug 2017; and after landfall at (g) 1400 and (h) 1900 UTC 26 Aug and (i) 0000 UTC 27 Aug 2017. The shaded contour represents the standard deviation of each term.

domains 3 and 4. Near the surface, the maximum azimuthally averaged tangential wind was over 30 m s^{-1} within a radius of 30–40 km from the storm center in domain 2, while it was less than 25 m s^{-1} in domains 1, 3, and 4.

For the hurricane inland, the height of maximum wind was about 1000 m for domain 1, 700 m for domain 2, and about 400 m for domains 3 and 4. High wind ($>35 \text{ m s}^{-1}$) extended up

to 3000 m in domains 3 and 4. Near the surface, the maximum azimuthally averaged tangential wind was over 10 m s^{-1} within a radius of 30–40 km from the storm center in domains 1 and 2, and less than 10 m s^{-1} in domains 3 and 4. At each time, the maximum wind speed was always at the lower level (approximately 400 m) in domain 3 and 4, in contrast to 1000 m in domains 1 and 2). Above the height of maximum wind, there

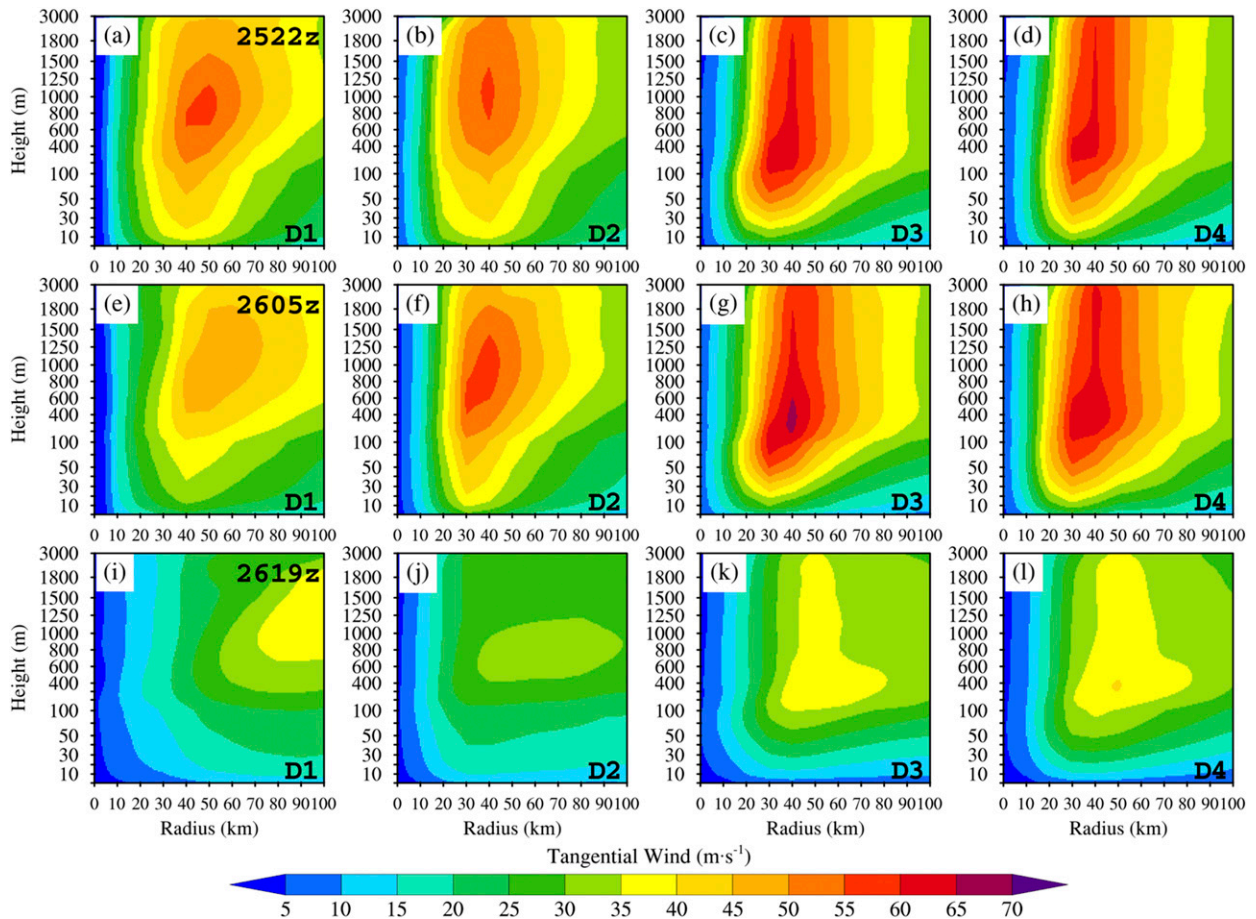


FIG. 6. Azimuthally averaged tangential wind from (a),(e),(i) domain 1, (b),(f),(j) domain 2, (c),(g),(k) domain 3, and (d),(h),(l) domain 4 for the hurricane (a)–(d) over the ocean at 2200 UTC 25 Aug, (e)–(h) during landfall at 0500 UTC 26 Aug, and (i)–(l) inland at 1900 UTC 26 Aug. D1, D2, D3, and D4 mark the simulation results from domains 1, 2, 3, and 4, respectively.

were significant upward trends for high wind in domains 3 and 4, extending upward over 2000 m. Near the surface, the wind in domains 1 and 2 tended to strongly mix with the high wind and always provided a higher maximum wind than in domains 3 and 4.

From Fig. 1b, domain 2 reproduced the intensity forecast matching the best track data, while the LES produced a higher 10 m maximum wind. Here, for the azimuthally averaged surface wind, domain 2 provided higher wind than LES. This contradiction may result from the differences between the YSU scheme and LES. The YSU scheme parameterizes turbulence eddies based on observations at a coarser resolution (compared to LES here) to adjust the maximum surface wind. In LES, smaller eddies were simulated, making the surface wind speed higher because of the strong eddies' strong mixing effect and lower because of the weak eddies' weak mixing effect. Compared to the total number of strong eddies, the number of weak eddies, typical in the atmosphere, was more extensive. Therefore, the azimuthally averaged surface wind speed was lower due to the larger number of weak eddies. The increase in weak surface wind preceded by weak eddies offset the smaller number of higher surface wind and finally resulted

in a lower azimuthally averaged surface wind. This weak azimuthally averaged surface wind was consistent with the weak maximum surface wind in domain 4 after filtering out the high wind preceded by strong eddies in Fig. 1b.

To investigate the reason for the difference in the tangential wind vertical structure between the simulation with the YSU scheme (in domains 1 and 2) and with LES (in domains 3 and 4), Fig. 7 shows the azimuthally averaged vertical flux for radial wind (positive for inflow) from all domains for the hurricane over the ocean at 2200 UTC 25 August (Figs. 7a–d), during landfall at 0500 UTC 26 August (Figs. 7e–h), and inland at 1900 UTC 26 August (Figs. 7i–l). Typically, in the Ekman layer (approximately the inflow layer in this study) where the flow is the result of a balance between the pressure gradient, Coriolis force, and turbulent drag forces, vertical inflow flux is key for the vertical structure of tangential wind (Kepert 2001).

Before landfall, there was negative flux in domains 1 and 2 below 200 m, with a minimum of less than $-1 \text{ m}^2 \text{ s}^{-2}$ and a positive flux above 400 m, with a maximum of over $1 \text{ m}^2 \text{ s}^{-2}$. For domain 3, because of the coarser (not fine enough) horizontal resolution, the LES model generated roll vortices with a larger width (all over 2.5 km), which is not accurate based on

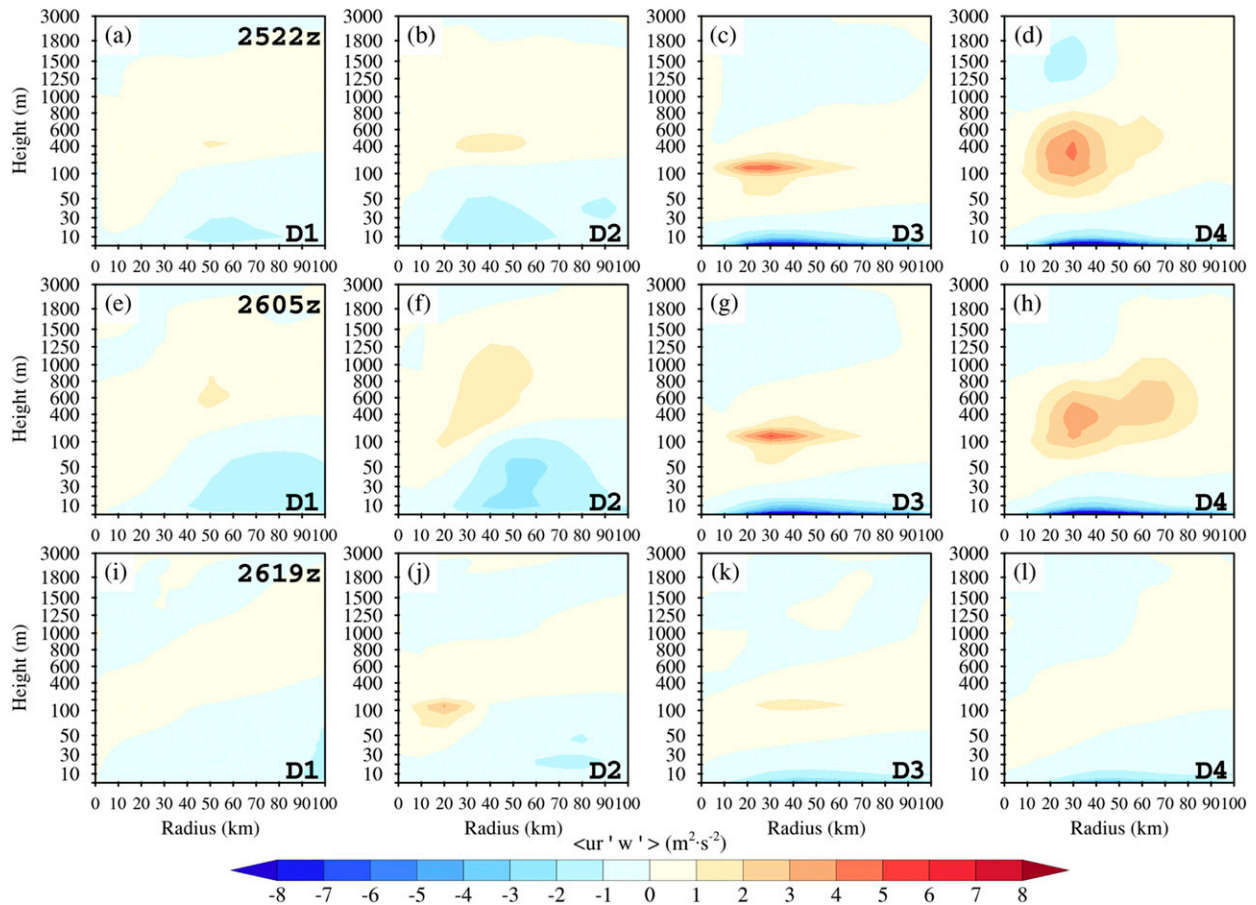


FIG. 7. As in Fig. 6, but for azimuthally averaged vertical flux for radial wind.

observations from Morrison et al. (2005). The two-dimensional Gaussian filter using the 5×5 bandwidth could not filter out the roll vortices in domain 3, allowing the flux induced by roll vortices to be zero. The flux in Fig. 7 for domain 3 was contributed mainly by subgrid-scale diffusion, which was strong at the height of about 10 m, leading to a momentum exchange that could mix the wind speed below 10 m. Therefore, the downward transport of high wind was controlled by the roll vortices. For domain 4, the negative flux was below 50 m, and above 50 m a strong positive flux extended up to 800 m, with a maximum of over $5 \text{ m}^2 \text{ s}^{-2}$. Above this positive flux, there was a weak negative flux at around 1000–2500 m.

During landfall, negative fluxes in domains 1 and 2 extended up to 200 m, with a minimum of less than -1 and $-2 \text{ m}^2 \text{ s}^{-2}$ for domains 1 and 2, respectively. For domain 4, the weak negative flux was still maintained below 50 m, and above 50 m the strong positive flux was reduced, with a maximum of over $4 \text{ m}^2 \text{ s}^{-2}$ and extending up to 800 m. Above this positive flux, the weak negative flux still existed, with a minimum of less than $-1 \text{ m}^2 \text{ s}^{-2}$. For the hurricane inland, the negative fluxes both weakened in all domains. For domain 4, strong azimuthally averaged positive flux generated by the roll vortices almost disappeared. However, this does not imply the disappearance of the roll vortices, and there should be some strong single roll,

as found by Wurman and Winslow (1998) and Morrison et al. (2005), that were eliminated by the azimuthally averaged analysis.

Combined with the azimuthally averaged tangential wind shown in Fig. 6, the strong positive flux (at around 400 m) in domain 4 first enhanced the Ekman layer's inflow. Consequently, it forced the tangential wind by the Coriolis force. This mechanism possibly explains the maximum tangential wind in domain 4 before (Fig. 6d) and during hurricane landfall (Fig. 6h). Similarly, the stronger negative flux (compared to that in domain 4) below 200 m in domain 2 could explain the near-surface higher wind. This stronger negative flux enhanced the mixing of inflow below 200 m and consequently increased the tangential wind by the Coriolis force. According to the revised MM5 surface layer scheme, the surface sensible heat and latent heat fluxes were proportional to the wind speed difference over land (which was zero) and at the first model level. Therefore, the greater surface wind in the model could lead to greater mixing of sensible and latent heat fluxes over the land surface. The larger energy transport enhanced the simulated hurricane in domains 1 and 2 (Fig. 2), and consequently the higher winds in domains 3 and 4, through the influences of the initial and boundary conditions. An in-depth analysis of the heat fluxes is provided in section 6.

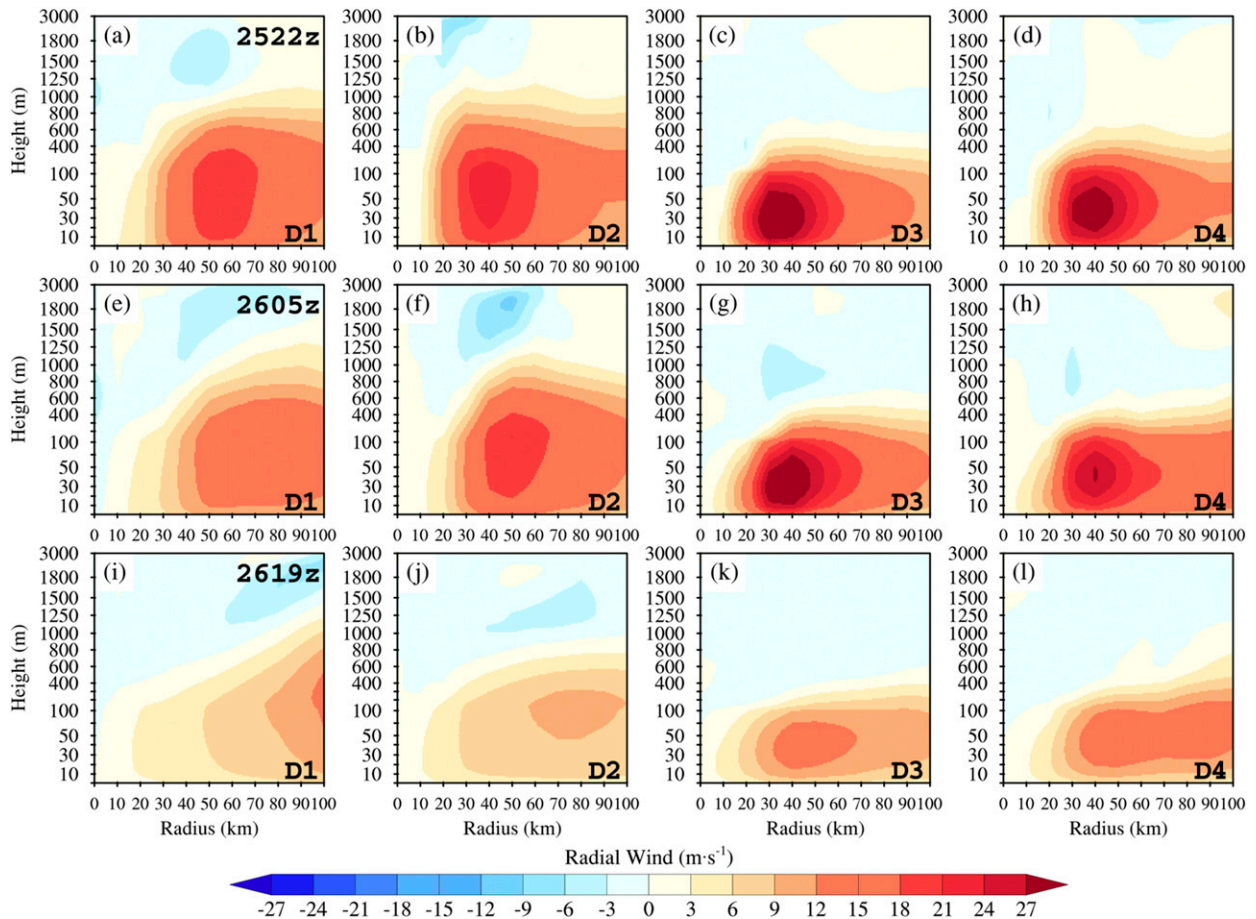


FIG. 8. As in Fig. 6, but for azimuthally averaged radial wind. Positive for inflow.

Finally, the higher near-surface wind was quickly reduced by the enhanced surface friction effect for the hurricane inland and led to the hurricane's rapid decay in domain 2. This is similar to Zhang et al. (2017), who found that strong vertical mixing was key in correcting the overestimated near-surface wind speed forecast. Here, we found that excessive vertical mixing can lead to underestimation of inland hurricane intensity.

b. Radial winds

For the evolution of radial wind, Fig. 8 shows the azimuthally averaged radial wind (positive for inflow) from all domains for the hurricane before landfall at 2200 UTC 25 August (Figs. 8a–d), during landfall at 0500 UTC (Figs. 8e–h), and after landfall at 1900 UTC 26 August (Figs. 8i–l). Before landfall, the maximum azimuthally averaged inflow was over 15 m s^{-1} for domain 1, 18 m s^{-1} for domain 2, and 27 m s^{-1} for both domains 3 and 4. The location height for these maxima was about 75 m in domains 1 and 2 and about 40 m in domains 3 and 4. The strong inflow ($>3 \text{ m s}^{-1}$) region extended up to 1000 m for domains 1 and 2 and to 600 m for domains 3 and 4. During landfall, the maximum azimuthally averaged inflow was over 12 m s^{-1} for domain 1, 15 m s^{-1} for domain 2, and

27 m s^{-1} for both domains 3 and 4. The location height for these maxima was about 75 m in domains 1 and 2 and about 40 m in domains 3 and 4. The strong inflow ($>3 \text{ m s}^{-1}$) region extended up to 1000 m for domains 1 and 2 and to 400 m for domains 3 and 4. After landfall, the maximum azimuthally averaged inflow was about 12 m s^{-1} in domain 1, 9 m s^{-1} in domain 2, and 12 m s^{-1} in both domains 3 and 4. The location height for these maxima in domains 1 and 2 was about 200 and 100 m, respectively, and about 40 m for domains 3 and 4. The strong inflow ($>3 \text{ m s}^{-1}$) region extended up to 1000 m for domain 1, to 600 m for domain 2, and to 400 m for domains 3 and 4. Compared to that in domains 3 and 4, the inflow was always deeper and weaker than that in domains 1 and 2. The extension of the inflow layer is consistent with the maximum tangential wind height. This agrees with Kepert and Wang (2001) and Zhang et al. (2011), who found that the height of the maximum wind was always located at the top of the Ekman layer (inflow layer). After landfall, the inflow was weakest in domain 2 in terms of magnitude and vertical extent, partially explaining the weak tangential winds seen in Fig. 6j.

To clarify the reason for the differences in the hurricane inflow vertical structure between the simulation with the coarser domains and with LES, Fig. 9 compares the azimuthally

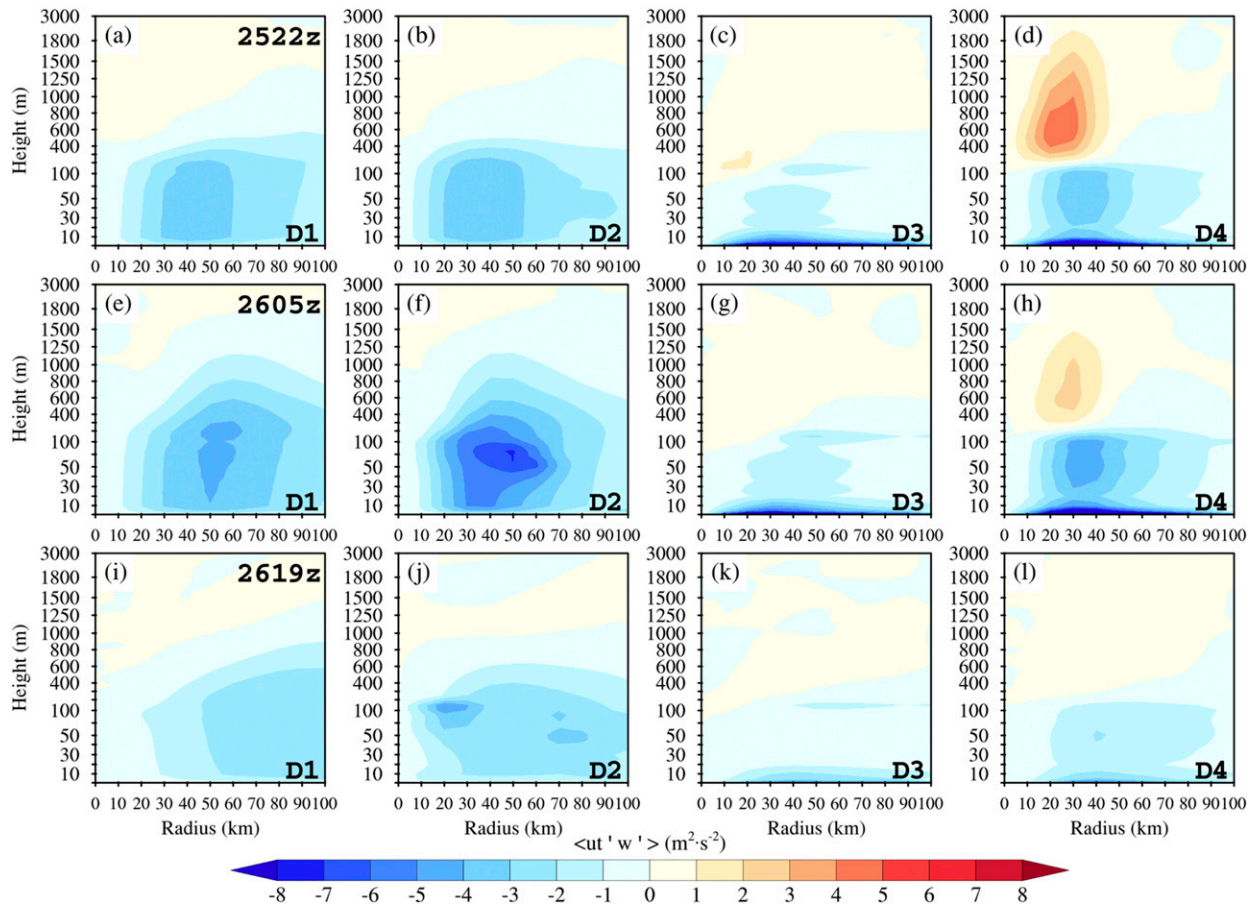


FIG. 9. As in Fig. 6, but for azimuthally averaged vertical flux for tangential wind.

averaged vertical flux for tangential wind from all domains for the hurricane over the ocean at 2200 UTC 25 August (Figs. 9a–d), during landfall at 0500 UTC 26 August (Figs. 9e–h), and inland at 1900 UTC 26 August (Figs. 9i–l). Before landfall, there were strong negative fluxes in domains 1 and 2 below 400 m. For domain 4, the strong negative flux was below 200 m, and above 200 m, a strong positive flux extended up to 2000 m. For domain 3, similarly, the flux induced by roll vortices was zero. The flux in Fig. 9 for domain 3 was contributed mainly by subgrid-scale diffusion. If the subgrid-scale diffusion flux in domain 3 is subtracted, the strongest negative flux produced by the roll vortices in domain 4 extends down to only 30 m, while the strongest negative flux in domains 1 and 2 extends to 3 m, the height of the first vertical level of the WRF Model in the numerical simulation.

During landfall, the strong negative fluxes extended up to 1000 m, with a minimum of $-4 \text{ m}^2 \text{ s}^{-2}$ for domain 1 and $-8 \text{ m}^2 \text{ s}^{-2}$ for domain 2. For domain 4, the strong negative flux induced by the roll vortices was still maintained below 200 m, and above 200 m the strong positive flux was reduced, with a maximum of over $3 \text{ m}^2 \text{ s}^{-2}$ and extending up to only 1600 m. If the subgrid-scale diffusion flux in domain 3 is subtracted, the strong negative flux ($-4 \text{ m}^2 \text{ s}^{-2}$) in domain 4 extends down to

only 20 m, while the strong negative flux ($-4 \text{ m}^2 \text{ s}^{-2}$) in domains 1 and 2 extends down to 3 m at the surface. For the hurricane inland, the strong negative fluxes weakened in domains 1 and 2, with a flux of $-2 \text{ m}^2 \text{ s}^{-2}$ at the surface. For domain 4, the negative flux generated by the roll vortices below 200 m was also weakened, and the strong positive flux disappeared. If the subgrid-scale diffusion flux in domain 3 is subtracted, the negative flux in domain 4 reaches only $-1 \text{ m}^2 \text{ s}^{-2}$ at the surface. Combined with the azimuthally averaged inflow in Fig. 8, the strong negative tangential flux produced by roll vortices could explain the stronger inflow in domain 4. The strong negative flux produced by roll vortices decreased the tangential wind first and consequently enhanced the inflow by way of a pressure gradient.

Above the Ekman layer ($>600 \text{ m}$), the strong positive tangential wind flux in domain 4 enhanced the tangential wind. Consequently, the Coriolis force from the enhanced tangential wind, which would lead to outflow, offset the enhanced inflow that was led by the positive flux (Figs. 7d,h) of radial wind at this level, suppressing the upward extension of the inflow layer that was led by the positive flux of radial wind. The vertical structure of high wind was finally formed as shown in Figs. 6d and 6h, consistent with the result in the ideal numerical

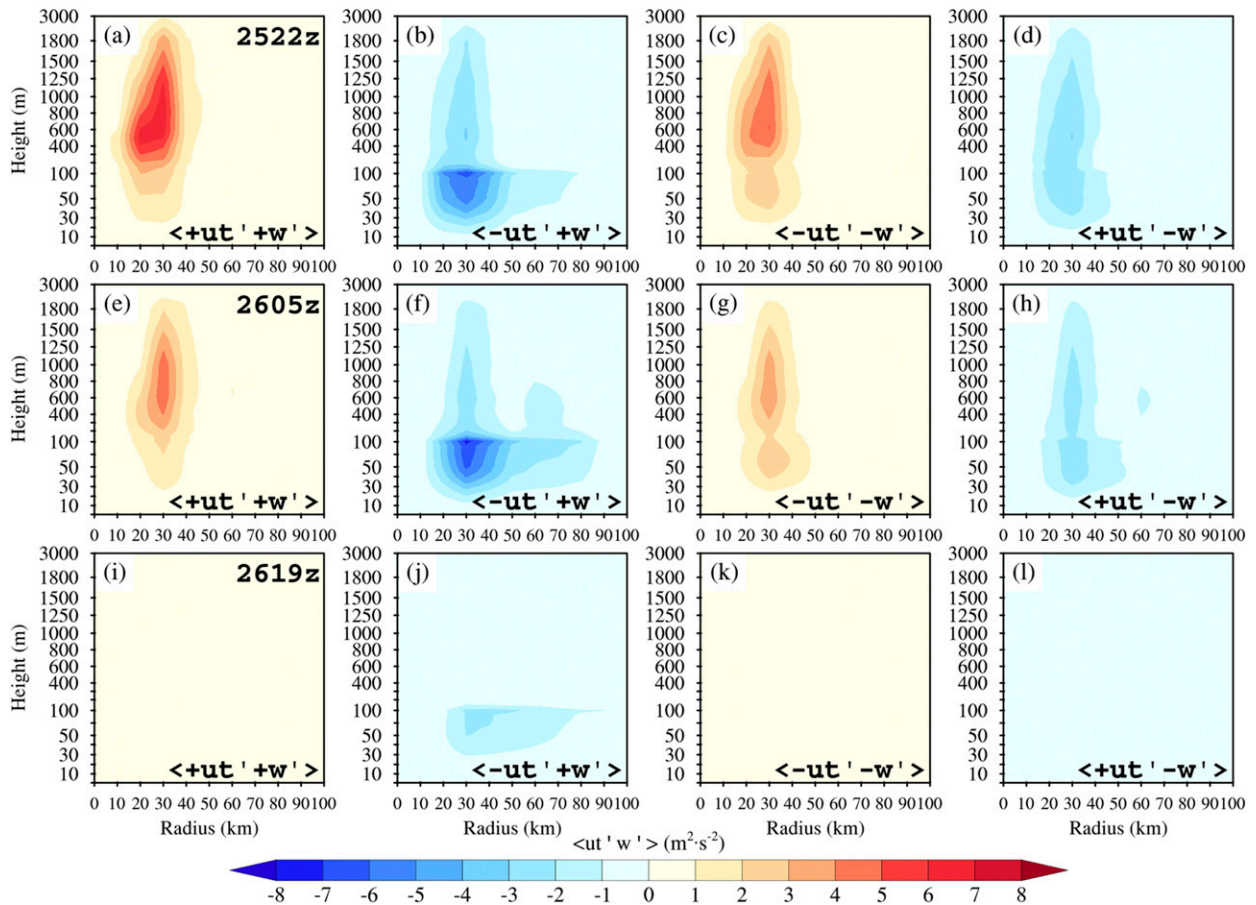


FIG. 10. Azimuthally averaged (a),(c),(e),(g),(i),(k) positive and (b),(d),(f),(h),(j),(l) negative tangential wind momentum fluxes induced by (a),(b),(e),(f),(i),(j) upward and (c),(d),(g),(h),(k),(l) downward turbulent motions for the hurricane (a)–(d) over the ocean at 2200 UTC 25 Aug, (e)–(h) during landfall at 0500 UTC 26 Aug, and (i)–(l) inland at 1900 UTC 26 Aug. The symbols “+” and “–” denote the positive and negative variables ut' and w' .

simulation by Gao and Ginis (2014, 2016, 2018) and Gao et al. (2017), who found that roll vortices can strongly influence the vertical structure of horizontal wind speed.

c. Upward and downward motion

According to the momentum flux analysis produced by the roll vortices (Figs. 7 and 9), it seems that the strong negative radial wind momentum flux at the lower level in domain 2 led to the higher azimuthally averaged wind and accelerated the decay of the hurricane in the simulated hurricane. However, from the net momentum flux analysis, it is not clear why the maxima of tangential and radial winds were both located at the lower height in the LESS. We speculate that upward and downward motion experienced by these roll vortices, as large eddies, may have had different contributions to the net flux and generated countergradient flux in the hurricane boundary layer (Gao and Ginis 2016). The flux component induced by this upward or downward turbulent motion was possibly more substantial, as it contributed to forming net momentum flux and eventually maintained the radial and tangential wind profiles in the LESS.

To clarify the contributions of the upward and downward motions, the net flux in domain 4 was divided into positive and negative fluxes with upward and downward motions as shown in Figs. 10 and 11. Figure 10 shows the azimuthally averaged positive (Figs. 10a,c,e,g,i,k) and negative (Figs. 10b,d,f,h,j,l) tangential wind vertical fluxes induced by upward (Figs. 10a,b,e,f,i,j) and downward (Figs. 10c,d,g,h,k,l) turbulent motions for the hurricane over the ocean at 2200 UTC 25 August (Figs. 10a–d), during landfall at 0500 UTC 26 August (Figs. 10e–h), and inland at 1900 UTC 26 August (Figs. 10i–l). Before landfall, the upward and downward turbulent motion generated not only positive but also negative flux from 20 to 3000 m. The strong negative flux below 200 m shown in Fig. 9d can be attributed mainly to the strong negative flux produced by the upward motion, with a minimum of less than $-8 \text{ m}^2 \text{ s}^{-2}$. The strong positive flux above 200 m shown in Fig. 9d can be attributed mainly to the upward motion, with a flux maximum of over $8 \text{ m}^2 \text{ s}^{-2}$.

During landfall, both the upward and downward turbulence motion also generated positive and negative flux from 20 to 1800 m. The strong negative flux below 200 m shown in Fig. 9h

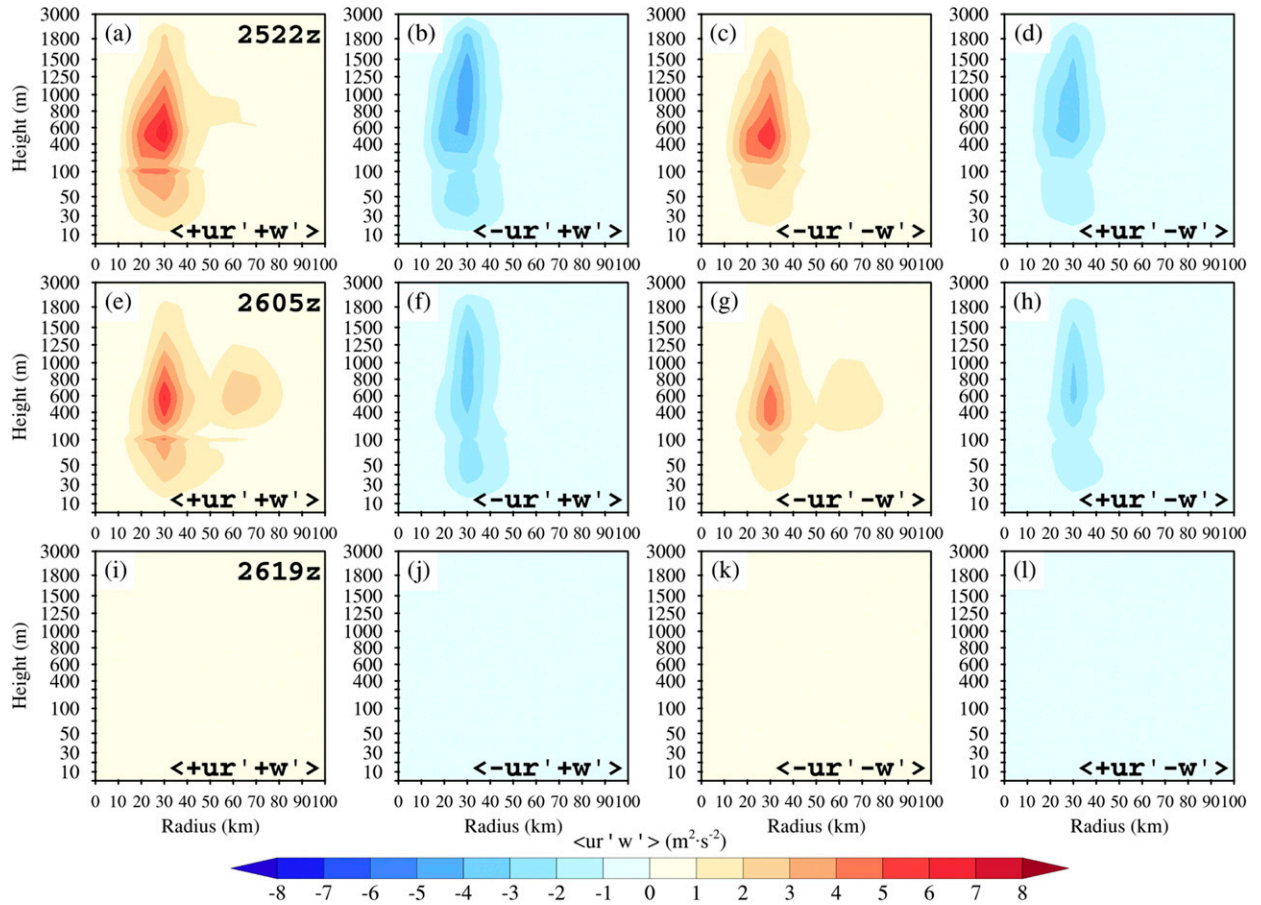


FIG. 11. As in Fig. 10, but for radial wind momentum flux. The symbols “+” and “−” denote the positive and negative variables ur' and w' .

can be attributed mainly to the upward motion, with a flux minimum of less than $-8 \text{ m}^2 \text{ s}^{-2}$. The strong positive flux above 200 m shown in Fig. 9h can be attributed to the almost equivalent upward and downward motion, with a flux maximum of over 4 and $3 \text{ m}^2 \text{ s}^{-2}$, respectively. For the hurricane inland, the positive flux was weak, and there was only a recognizable negative flux produced by the upward motion at 30 to 200 m. Based on these results, we can conclude that the roll vortices generated not only positive but also negative vertical flux during the simulation period. Below 200 m, the positive flux suppressed the downward mixing of tangential wind produced by the excessively strong negative flux. Then, this weak tangential wind led to a weak Coriolis force that maintained the inflow in domain 4 for the hurricane inland. Above 400 m, the positive flux completely suppressed the negative flux preceded by the roll vortices and finally forced the inflow to extend below 400 m in the LES. Meanwhile, the negative flux (above the Ekman layer) suppressed the upward movement of maximum wind produced by the excessively strong positive flux. Finally, this suppression mechanism maintained the maximum tangential wind at around 400 m.

Figure 11 shows the azimuthally averaged positive (Figs. 11a,c,e,g,i,k) and negative (Figs. 11b,d,f,h,j,l) radial wind

vertical flux for upward (Figs. 11a,b,e,f,i,j) and downward (Figs. 11c,d,g,h,k,l) turbulence motion for the hurricane over the ocean at 2200 UTC 25 August (Figs. 11a–d), during landfall at 0500 UTC 26 August (Figs. 11e–h), and inland at 1900 UTC 26 August (Figs. 11i–l). Similar to the tangential wind vertical flux, before landfall, the upward and downward turbulence motion generated not only positive but also negative flux from 20 to 3000 m. The weak negative flux below 40 m shown in Fig. 7d can be attributed to the almost equivalent positive and negative flux produced by the upward and downward motion of roll vortices. The strong positive flux above 50 m shown in Fig. 7d can be attributed to the upward and downward motion, with a flux maximum of over 6 and $5 \text{ m}^2 \text{ s}^{-2}$, respectively. Above the height of positive flux in Fig. 7d, the negative flux produced by the upward and downward motion controlled the net flux and made it negative. During landfall, the weak negative flux below 40 m shown in Fig. 7h can be attributed to the almost equivalent positive and negative flux produced by the roll vortices. The strong positive flux above 50 m shown in Fig. 7h can be attributed to the upward and downward motion, with a flux maximum of over 5 and $4 \text{ m}^2 \text{ s}^{-2}$, respectively. Above the height of positive flux in Fig. 7h, the negative flux produced by the upward and downward motion controlled the net flux and made it negative. For the hurricane inland, the

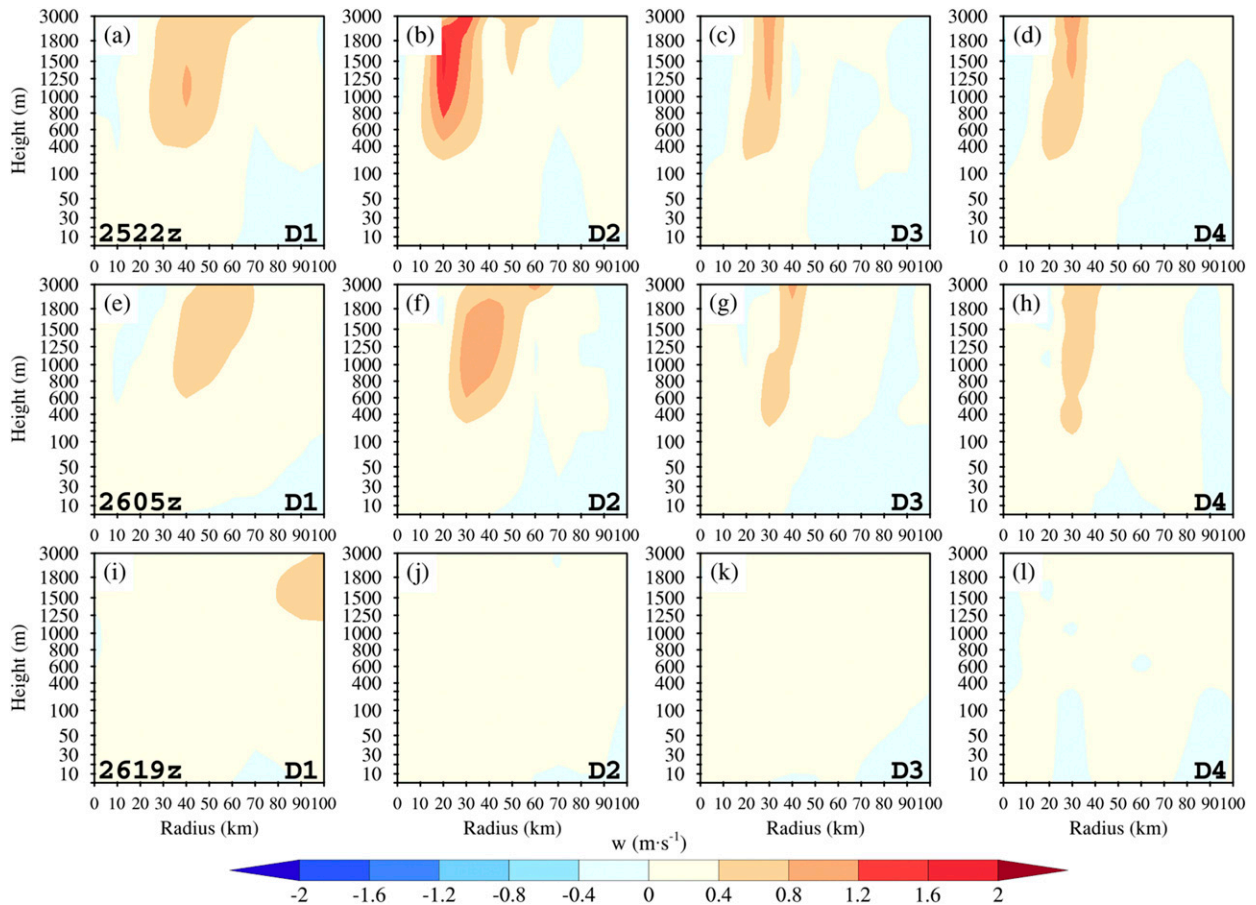


FIG. 12. As in Fig. 6, but for azimuthally averaged vertical velocity.

positive and negative flux both weakened. Because of the approximate magnitude of the positive and negative flux generated by the upward and downward turbulence motion, the negative flux below 50 m and above 1000 m was weak during the simulation period. The more substantial positive flux from both the upward and downward motion provided the positive flux in Fig. 7. The negative flux, which was weaker than that in the YSU scheme, led to the weak surface tangential wind by the weak Coriolis force and finally weakened the reduction effect by land surface friction in the LES-simulated hurricane after landfall (Fig. 6). In addition, there is no strong negative flux near the surface in Figs. 10 and 11, which confirms that subgrid-scale diffusion generated the near-surface flux in Figs. 7 and 9.

5. The effects of roll vortices on precipitation

As shown in Fig. 3, the simulations from the coarser domains (e.g., domains 1 and 2) and LES produced different precipitation amounts during the simulation period. To examine the effect of roll vortices on precipitation, vertical velocity, and water vapor supplies in and near the hurricane eyewall are analyzed in this section.

Figure 12 shows the azimuthally averaged vertical velocity from all domains for the hurricane over the ocean at 2200 UTC

25 August (Figs. 12a–d), during landfall at 0500 UTC 26 August (Figs. 12e–h), and inland at 1900 UTC 26 August (Figs. 12i–l). To compare with the flux produced by the roll vortices, we considered only the updraft below 3000 m. Before landfall, the maximum for azimuthally averaged updraft was over 0.8, 1.6, 0.8, and 1.2 m s^{-1} for the simulation in domains 1, 2, 3, and 4, respectively. During landfall, the maximum for azimuthally averaged updraft was over 0.4, 0.8, 0.8, and 0.4 m s^{-1} for the simulation in domains 1, 2, 3, and 4, respectively. For the hurricane inland, the updraft almost disappeared in domains 2–4, with a maximum of less than 0.4 m s^{-1} . The stronger azimuthally averaged updraft in domain 2 before landfall may be associated with the overestimated heavy rain for the hurricane over the ocean, as shown in Fig. 3. That is, the updraft was an important reason for heavy rain. For domain 1, even with a weak azimuthally averaged updraft, it still generated unrealistic heavy rain before hurricane landfall, implying that the updraft was not the only cause. The vertical moisture flux can explain the overestimated precipitation in domain 1, as discussed at the end of the section.

Vertical motion commonly depends on the thermodynamic conditions in the atmosphere. To explore the reason for the different updrafts in the four domains, we turn to temperature

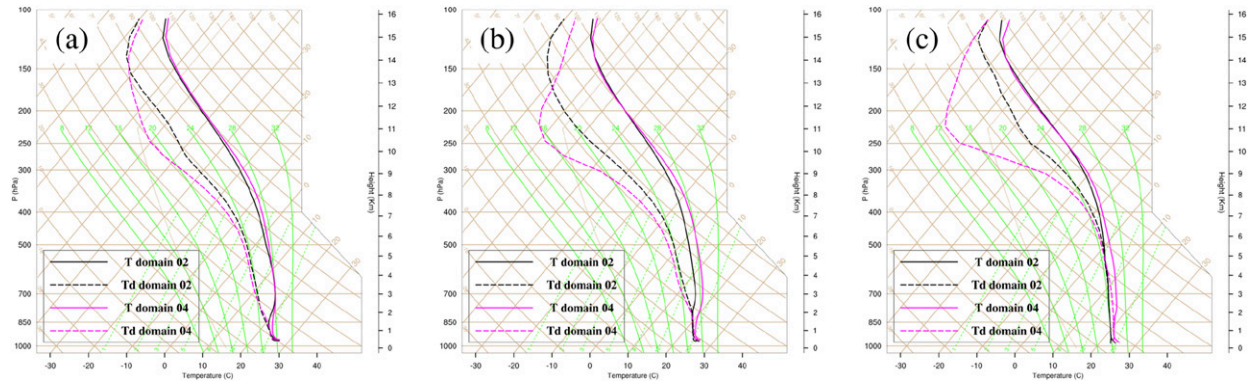


FIG. 13. Skew T -log p diagram for averaged temperature within a radius of 10–40 km in domain 2 (black line) and domain 4 (magenta line) for the hurricane (a) over the ocean at 2200 UTC 25 Aug, (b) during landfall at 0500 UTC 26 Aug, and (c) inland at 1900 UTC 27 Aug 2017.

stratifications in the different simulations. Considering that the updraft usually occurred around a radius of 10–40 km from the storm center, a skew T -log p diagram for the average temperature within a radius of 10–40 km in domains 2 and 4 is shown in Fig. 13 for the hurricane over the ocean (Fig. 13a), at landfall (Fig. 13b), and inland (Fig. 13c). Before and during landfall, the temperature in domain 4 was higher than that in domain 2 below 3 km. The cooling rate was greater than the moist adiabatic cooling rate in domain 2, and less than the moist adiabatic cooling rate in domain 4. Due to the high humidity below 1 km, the low-level CAPE in domain 2 was larger than that in domain 4. Therefore, the larger CAPE led to a stronger azimuthally averaged updraft in domain 2 and finally to stronger unrealistic precipitation. For the hurricane inland, the temperature in domain 4 was also greater than that in domain 2 below 3 km. The cooling rate in domain 2 was close to the moist adiabatic cooling rate, while the cooling rate in domain 4 was still less than the moist adiabatic cooling rate below 2 km. The thermal stratification against the upward motion in domains 2 and 4 finally led to weak precipitation inland.

The analysis of thermal stratification indicates that different temperature profiles led to the different updrafts in domains 2 and 4. To clarify the effect of the roll vortices, Fig. 14 shows the azimuthally averaged virtual potential temperature flux from all domains for the hurricane over the ocean at 2200 UTC 25 August (Figs. 14a–d), during landfall at 0500 UTC 26 August (Figs. 14e–h), and inland at 1900 UTC 26 August (Figs. 14i–l). The azimuthally averaged tangential wind vertical flux from the roll vortices was also added in domain 4 as a contour line to distinguish the roll vortices and other turbulence. Similar to the other fluxes discussed above, the flux in domain 3 can be attributed mainly to subgrid-scale diffusion. Before landfall, the positive flux below 200 m was similar in domains 1, 2, and 4, with a maximum of over 0.2 K m s^{-2} . Above 200 m, there was a strong negative flux, with a minimum of less than -0.8 K m s^{-2} produced by the roll vortices in domain 4, while the entrainment process generated a weak negative flux in domains 1 and 2. The strong negative flux strongly mixed the temperature vertically and provided a low vertical

cooling rate in domain 4. The weak negative flux provided an overmoist adiabatic cooling rate in domain 2. During landfall, the entrainment was strong and led to a strong negative flux, with a minimum of less than -0.8 K m s^{-2} , and a decrease in the vertical cooling rate in domain 2. For the hurricane inland, the entrainment process remained with a minimum of -0.3 K m s^{-2} , and it continued to decrease the vertical cooling rate in domain 2. In domain 4, the negative flux produced by the roll vortices almost disappeared. During the whole simulation period, we found that the roll vortices caused the increased temperature at the lower level and finally led to a weak azimuthally averaged updraft and weak rain rates, while the simulations with the YSU scheme underestimated the temperature, generated a strong azimuthally averaged updraft, and overestimated the precipitation for the hurricane over the ocean.

However, the reason for the higher temperature at the higher level in domain 4, and for the heavy rain in domain 1 of the hurricane over the ocean, is still not clear. To investigate the causes, Fig. 15 shows the azimuthally averaged water vapor flux in all domains for the hurricane over the ocean at 2200 UTC 25 August (Figs. 15a–d), during landfall at 0500 UTC 26 August (Figs. 15e–h), and inland at 1900 UTC 26 August (Figs. 15i–l). The azimuthally averaged tangential wind vertical flux from the roll vortices was also added in domain 4 as a contour line to distinguish the roll vortices and other turbulence. Similarly, the flux in domain 3 can be attributed mainly to subgrid-scale diffusion. Before landfall, the strong positive flux extended up to 600 m in domains 1 and 2, with a maximum of over 0.4 and $0.5 \text{ g m s}^{-1} \text{ kg}^{-1}$, respectively. Considering that the updraft usually started at the height of 200 m, this strong water vapor support in domains 1 and 2 could lead to heavy rain at this stage. Especially for domain 1, sufficient water vapor support was the leading factor for the heavy rainfall over the ocean. For domain 4, the roll vortices produced a positive flux below 200 m, with a maximum of over $0.4 \text{ g m s}^{-1} \text{ kg}^{-1}$. Above 100 m, there was obviously no flux produced by roll vortices, and most fluxes can be attributed to cloud turbulence. The positive flux produced by cloud turbulence would increase the temperature by the latent heat of

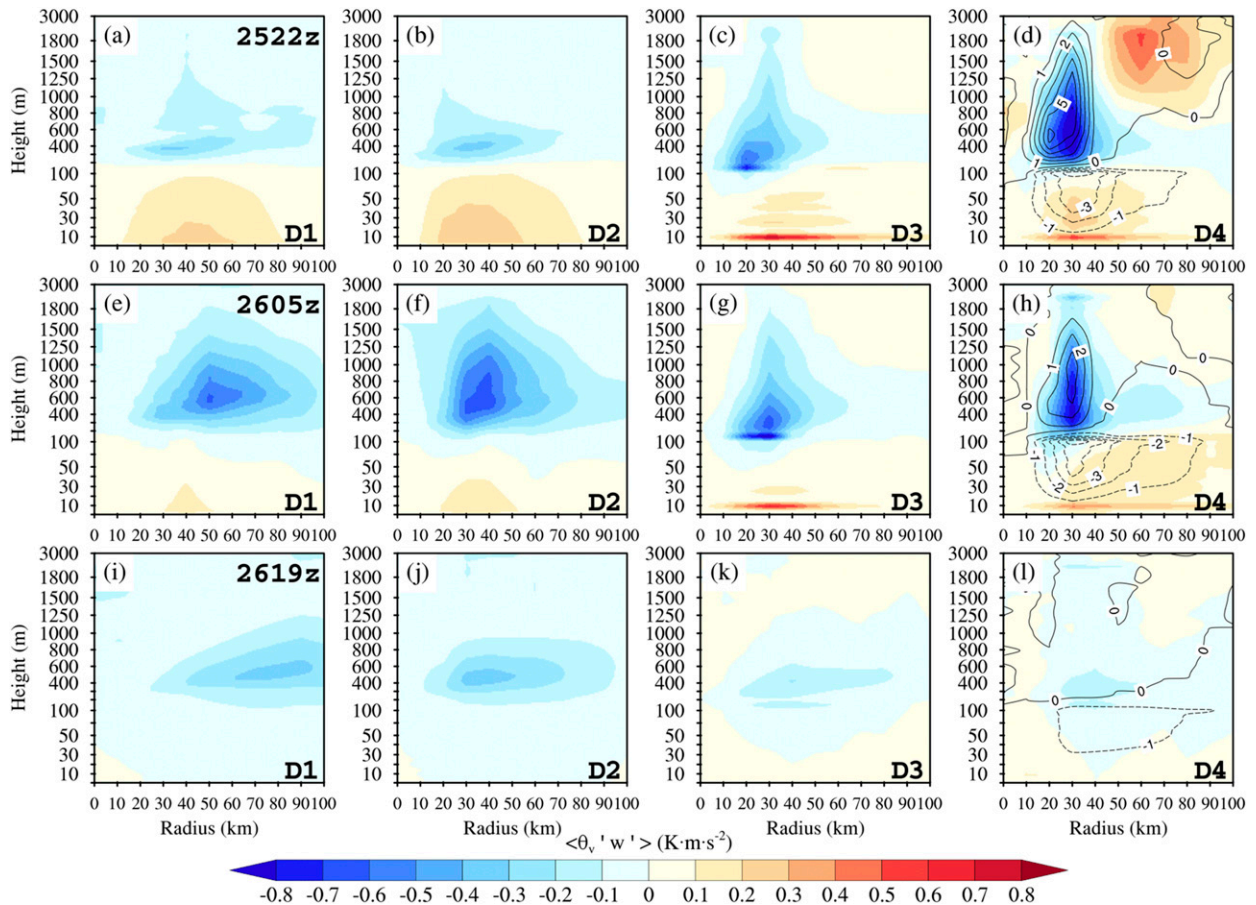


FIG. 14. As in Fig. 6, but for azimuthally averaged virtual potential temperature flux. (d),(h),(l) The related azimuthally averaged tangential wind momentum flux from roll vortices is added as a contour line. D1, D2, D3, and D4 denote the simulation results from domains 1, 2, 3, and 4, respectively.

condensation. Then the roll vortices transported the warm air downward and led to the stable stratifications in domain 4. This insufficient water vapor support, as well as stable thermodynamic conditions, made the LES generate weaker rainfall for the hurricane over the ocean. During landfall, the positive flux extended up to 1200 m in domains 1 and 2, with a maximum of over 0.3 and $0.4 \text{ g m s}^{-1} \text{ kg}^{-1}$, respectively. For domain 4, the roll vortices introduced positive flux below 200 m. For the hurricane inland, the positive flux was weak in domains 1 and 2, with a maximum of less than 0.3 and $0.2 \text{ g m s}^{-1} \text{ kg}^{-1}$, respectively. The strong positive flux in domain 4 almost disappeared, with a maximum of less than $0.1 \text{ g m s}^{-1} \text{ kg}^{-1}$. This weak water vapor flux supported the reduction of the substantial rainfall in the simulation, consistent with the stage IV data, which showed the rain gradually weakening at 1200 26 August in Fig. 3a.

6. Vertical eddy diffusivity and latent and sensible heat fluxes

Based on the analysis of momentum flux preceded by the roll vortices, we know that the strong negative momentum flux at

the lower level (below 100 m in Fig. 7) in the simulation with the YSU scheme could lead to the higher azimuthally averaged wind in the simulated hurricane. Considering that momentum flux is controlled by the eddy diffusion coefficient of momentum (K_m) in the YSU scheme, according to the Monin–Obukhov (M–O) similarity theory, K_m indicates the turbulence eddy mixing effect between different levels. A larger K_m indicates stronger mixing for variables (Zhang and Pu 2017). Therefore, K_m could be used in a sensitivity study to confirm the impact of strong negative momentum at the lower level (below 100 m in Figs. 6 and 8). Therefore, a sensitivity experiment (referred to as Sexp hereafter) was set up based on domains 1 and 2 only, with K_m set at half the original K_m below 100 m. The simulation outcomes were compared with the results with the original K_m . Figure 16 compares the evolution of azimuthally averaged surface sensible and latent heat fluxes between the original and Sexp simulations. We found that the maximum of surface sensible and latent heat fluxes occurred at approximately 0000 UTC 26 August 2017 in both the original and sensitivity simulations. For azimuthally averaged surface sensible heat fluxes, the maximum was 180 W m^{-2} for the original domain 1, 260

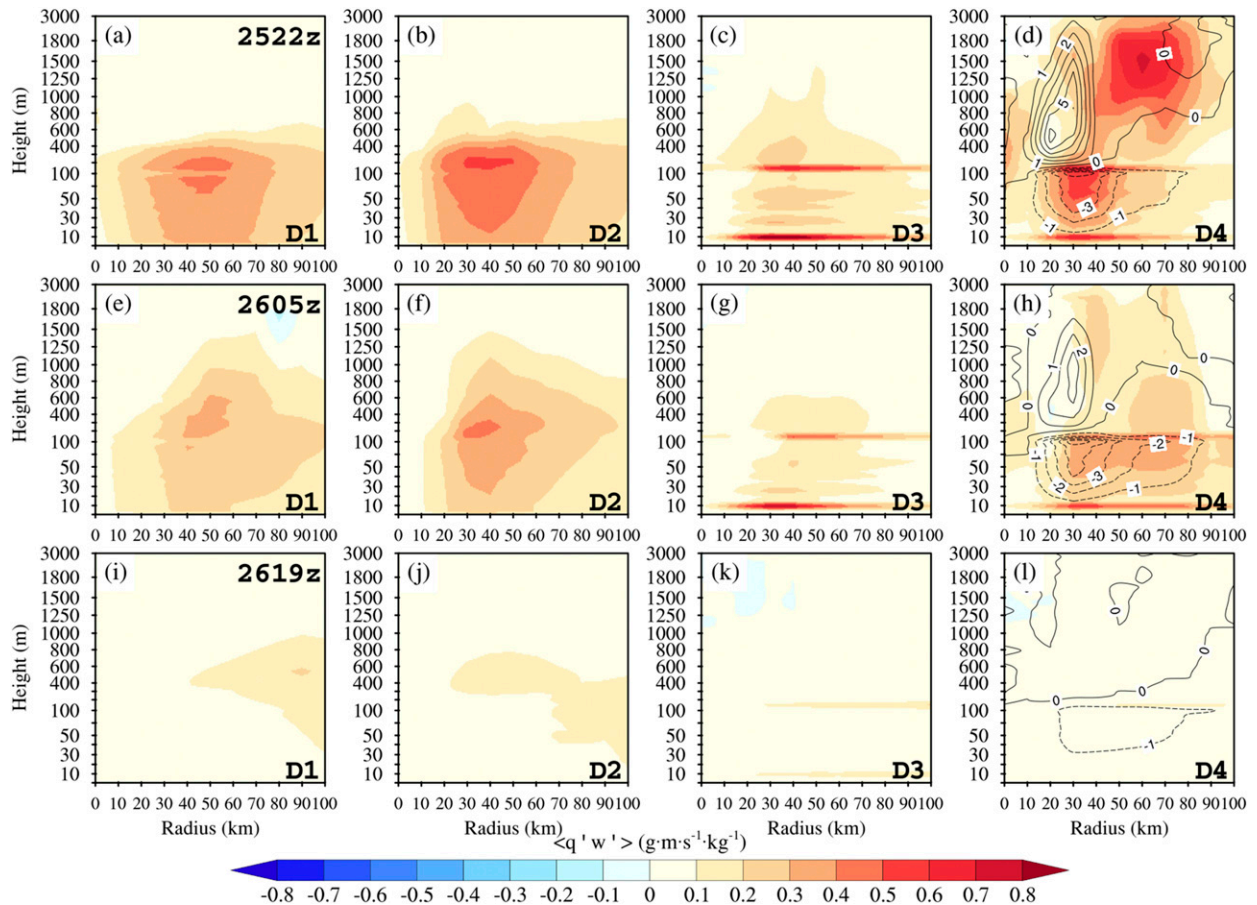


FIG. 15. As in Fig. 6, but for azimuthally averaged water vapor flux. (d),(h),(l) The related azimuthally averaged tangential wind momentum flux from roll vortices is added as a contour line. D1, D2, D3, and D4 denote the simulation results from domains 1, 2, 3, and 4, respectively.

W m^{-2} for the original domain 2, 120 W m^{-2} for Sexp domain 1, and 180 W m^{-2} for Sexp domain 2. For azimuthally averaged surface latent heat fluxes, the maximum was 800 W m^{-2} for the original domain 1, 1100 W m^{-2} for the original domain 2, 600 W m^{-2} for Sexp domain 1, and 800 W m^{-2} for Sexp domain 2. Obviously, the surface sensible and latent heat fluxes were all reduced in the Sexp simulation. With the smaller momentum eddy diffusion coefficient ($1/2$ of the original Km) below 100 m , the sensitivity simulation led to weak surface energy support.

To verify the influence of this weak energy support on the hurricane winds, Fig. 17 shows the azimuthally averaged wind speed from the original domain 1 (Figs. 17a,e,i), original domain 2 (Figs. 17b,f,j), Sexp domain 1 (Figs. 17c,g,k), and Sexp domain 2 (Figs. 17d,h,l) for the hurricane before intensification at 1200 UTC 25 August (Figs. 17a–d), after intensification at 0000 UTC 26 August (Figs. 17e–h), and inland at 1800 UTC 26 August (Figs. 17i–l). Before intensification, the maximum of azimuthally averaged wind speed was over 45 m s^{-1} for the simulation in the original domain 1, 50 m s^{-1} in the original domain 2, 40 m s^{-1} in Sexp domain 1, and 45 m s^{-1} in Sexp domain 2. After intensification, the maximum azimuthally

averaged wind speed was over 55 m s^{-1} for the simulation in the original domain 1, 60 m s^{-1} in the original domain 2, 50 m s^{-1} in Sexp domain 1, and 60 m s^{-1} in Sexp domain 2. For the hurricane inland, the maximum azimuthally averaged wind speed was over 35 m s^{-1} for the simulation in the original domain 1, 30 m s^{-1} in the original domain 2, 40 m s^{-1} in Sexp domain 1, and 35 m s^{-1} in Sexp domain 2. We found that before landfall, the Sexp simulation often showed a weak hurricane with weak maximum wind speed. Although the maximum wind speed in Sexp domain 2 was equal to that in the original domain 2 after intensification, the region of maximum wind speed was smaller in Sexp domain 2 than in the original domain 2. After landfall, the Sexp simulation showed a stronger hurricane with higher maximum wind speed. As we found above, the strong negative flux at the lower level enhanced the energy support from the surface for the hurricane over the ocean, and the weak negative flux produced by the smaller Km could lead to weak energy support (see in Fig. 16), and finally a weak hurricane with lower maximum wind speed. For the hurricane inland, the strong negative momentum flux in the original simulation could quickly destroy the inflow and finally accelerate the decay of the hurricane. For the Sexp

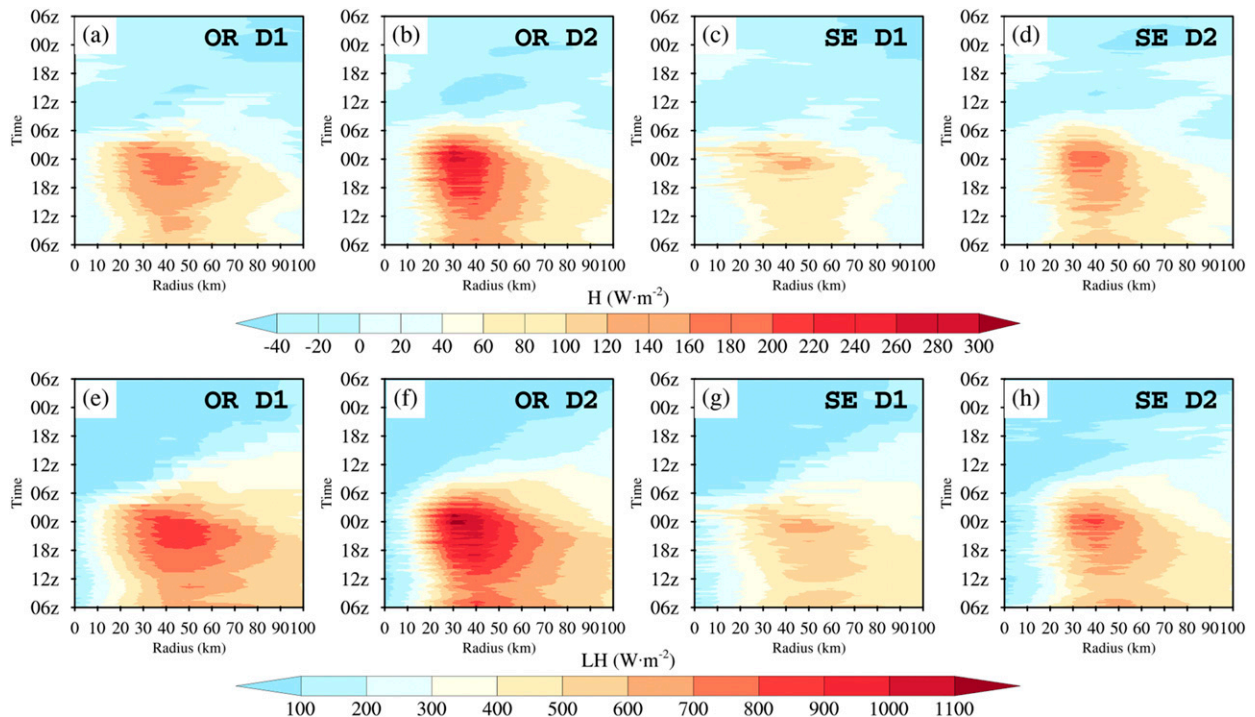


FIG. 16. Evolution of azimuthally averaged (a)–(d) surface sensible heat flux and (e)–(h) latent heat flux from the original (a),(e) domain 1, (b),(f) domain 2, sensitivity simulation in (c),(g) domain 1, and (d),(h) domain 2. OR and SE represent the original and sensitivity simulation results. D1 and D2 denote the simulation results from domains 1 and 2, respectively.

simulation, the weak negative flux produced by the smaller Km slowed the decay of the hurricane and provided a higher maximum wind speed. Overall, the sensitivity experiment confirms the significant impact of the strong negative momentum flux at the lower level in the simulation with the YSU scheme. It enhanced the hurricane before landfall but accelerated its decay after landfall.

7. Summary

In this paper, a one-way nested WRF-LES model was used to explore the effect of roll vortices on the evolution of Hurricane Harvey during its landfall from 0000 UTC 25 August to 1800 UTC 27 August 2017. The simulation results indicate that the roll vortices prevailed and controlled the turbulence in the LESSs. Simulation verification indicated that the LES provided better hurricane wind vertical structure and precipitation simulations over the ocean. The intensity simulated with LES was consistent with the high temporal resolution observations from Wurman and Kosiba (2018) and Fernández-Cabán et al. (2019) and indicates a good simulation result. The simulation with the YSU PBL scheme overestimated the precipitation for the hurricane over the ocean.

During the simulation period, the roll vortices introduced net positive momentum tangential flux, transported high wind upward, and thinned the inflow layer. The negative momentum flux produced by roll vortices suppressed

the maximum wind vertical transport and maintained it at around 400 m, in contrast to 1000 m in the YSU-driven simulation. During landfall, the weak negative flux maintained the higher wind in the LESSs, while the low-level strong negative flux in the coarser domains with the YSU PBL scheme enhanced the surface energy support and led to an unrealistic strong hurricane but accelerated its decay during landfall. Meanwhile, the roll vortices caused the increased temperature and drier air at the lower level and thus also led to a weak updraft, which combined with insufficient water vapor support and eventually generated weaker rainfall closer to observations for the hurricane over the ocean.

In addition, the YSU scheme was used at 2.5 km horizontal grid spacing in this study. Although previous studies indicated that the YSU scheme performs better with horizontal grid spacing of 1–2 km (Fierro et al. 2009; Nolan et al. 2009; Gentry and Lackmann 2010) than with coarser grids, the major improvement of higher resolution is on the horizontal structure. Since impact of roll vortices is mainly in the vertical flux contribution (Gao and Ginis 2014, 2016, 2018), the horizontal grid spacing of 2.5 km is sufficient for comparing the simulations with YSU and LES in this study. Future studies could use the YSU scheme at a horizontal resolution of 1–2 km for further evaluation. Moreover, future work should further explore the dynamic mechanisms and energy processes associated with roll vortices for landfalling hurricanes with more case studies.

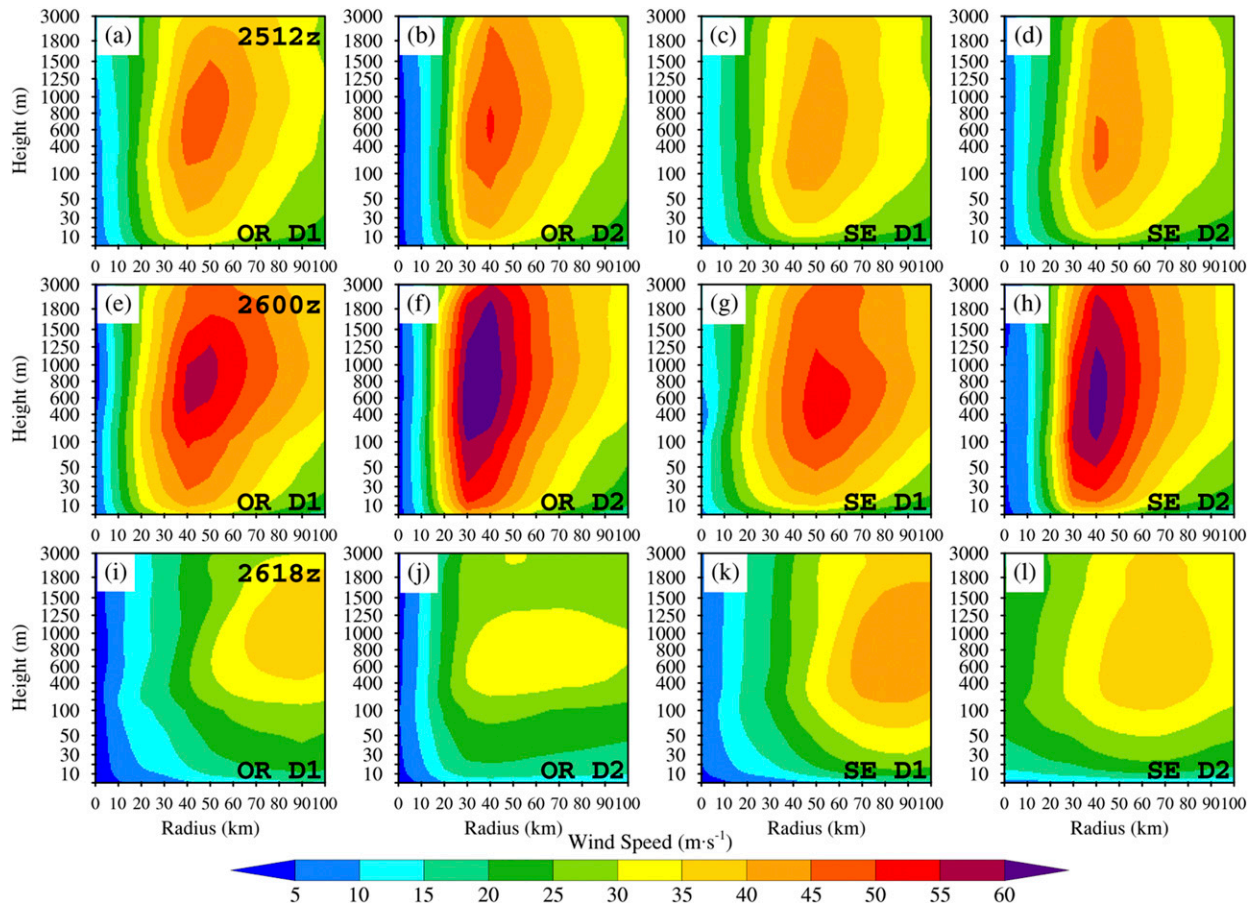


FIG. 17. Azimuthally averaged wind speed from the (a),(e),(i) original domain 1, (b),(f),(j) original domain 2, (c),(g),(k) sensitivity domain 1, and (d),(h),(l) sensitivity domain 2 for the hurricane (a)–(d) before intensification at 1200 UTC 25 Aug, (e)–(h) after intensification at 0000 UTC 26 Aug, and (i)–(l) inland at 1800 UTC 26 Aug. OR and SE represent the original and sensitivity simulation results. D1 and D2 denote the simulation results from domains 1 and 2, respectively.

Acknowledgments. This study was supported by NSF Grants ECCS-1839833 (ZP and XL) and OAC-2004658 (ZP) and NOAA Award NA19OAR4590239 (ZP and XL). The computational resources from the UCAR CISL supercomputing system are appreciated. The NOAA Hurricane Research Division (HRD) radar wind analysis (https://www.aoml.noaa.gov/hrd/data_sub/radar.html) and the NCEP stage IV precipitation analysis (Lin and Mitchell 2005) were used for verification. Review comments from three anonymous reviewers are appreciated.

REFERENCES

- Alford, A. A., M. I. Biggerstaff, G. D. Carrie, J. L. Schroeder, B. D. Hirth, and S. M. Waugh, 2019: Near-surface maximum winds during the landfall of Hurricane Harvey. *Geophys. Res. Lett.*, **46**, 973–982, <https://doi.org/10.1029/2018GL080013>.
- Brown, R. A., 1980: Longitudinal instabilities and secondary flows in the planetary boundary layer: A review. *Rev. Geophys.*, **18**, 683–697, <https://doi.org/10.1029/RG018i003p00683>.
- Chen, F., and J. Dudhia, 2001: Coupling an advanced land surface–hydrology model with the Penn State–NCAR MM5 modeling system. Part I: Model implementation and sensitivity. *Mon. Wea. Rev.*, **129**, 569–585, [https://doi.org/10.1175/1520-0493\(2001\)129<0569:CAALSH>2.0.CO;2](https://doi.org/10.1175/1520-0493(2001)129<0569:CAALSH>2.0.CO;2).
- Dudhia, J., 1989: Numerical study of convection observed during the Winter Monsoon Experiment using a mesoscale two-dimensional model. *J. Atmos. Sci.*, **46**, 3077–3107, [https://doi.org/10.1175/1520-0469\(1989\)046<3077:NSOCOD>2.0.CO;2](https://doi.org/10.1175/1520-0469(1989)046<3077:NSOCOD>2.0.CO;2).
- Ellis, R., and S. Businger, 2010: Helical circulations in the typhoon boundary layer. *J. Geophys. Res.*, **115**, D06205, <https://doi.org/10.1029/2009JD011819>.
- Etling, D., and R. A. Brown, 1993: Roll vortices in the planetary boundary layer: A review. *Bound.-Layer Meteor.*, **65**, 215–248, <https://doi.org/10.1007/BF00705527>.
- Fernández-Cabán, P. L., and Coauthors, 2019: Observing Hurricane Harvey’s eyewall at landfall. *Bull. Amer. Meteor. Soc.*, **100**, 759–775, <https://doi.org/10.1175/BAMS-D-17-0237.1>.
- Fierro, A. O., R. F. Rogers, F. D. Marks, and D. S. Nolan, 2009: The impact of horizontal grid spacing on the microphysical and kinematic structures of strong tropical cyclones simulated with the WRF-ARW model. *Mon. Wea. Rev.*, **137**, 3717–3743, <https://doi.org/10.1175/2009MWR2946.1>.
- Foster, R. C., 2005: Why rolls are prevalent in the hurricane boundary layer. *J. Atmos. Sci.*, **62**, 2647–2661, <https://doi.org/10.1175/JAS3475.1>.

- Gao, K., and I. Ginis, 2014: On the generation of roll vortices due to the inflection point instability of the hurricane boundary layer flow. *J. Atmos. Sci.*, **71**, 4292–4307, <https://doi.org/10.1175/JAS-D-13-0362.1>.
- , and —, 2016: On the equilibrium-state roll vortices and their effects in the hurricane boundary layer. *J. Atmos. Sci.*, **73**, 1205–1222, <https://doi.org/10.1175/JAS-D-15-0089.1>.
- , and —, 2018: On the characteristics of linear-phase roll vortices under a moving hurricane boundary layer. *J. Atmos. Sci.*, **75**, 2589–2598, <https://doi.org/10.1175/JAS-D-17-0363.1>.
- , —, J. D. Doyle, and Y. Jin, 2017: Effect of boundary layer roll vortices on the development of an axisymmetric tropical cyclone. *J. Atmos. Sci.*, **74**, 2737–2759, <https://doi.org/10.1175/JAS-D-16-0222.1>.
- Gentry, M. S., and G. M. Lackmann, 2010: Sensitivity of simulated tropical cyclone structure and intensity to horizontal resolution. *Mon. Wea. Rev.*, **138**, 688–704, <https://doi.org/10.1175/2009MWR2976.1>.
- Hong, S. Y., 2010: A new stable boundary-layer mixing scheme and its impact on the simulated East Asian summer monsoon. *Quart. J. Roy. Meteor. Soc.*, **136**, 1481–1496, <https://doi.org/10.1002/qj.665>.
- , Y. Noh, and J. Dudhia, 2006: A new vertical diffusion package with an explicit treatment of entrainment processes. *Mon. Wea. Rev.*, **134**, 2318–2341, <https://doi.org/10.1175/MWR3199.1>.
- Huang, L., X. Li, B. Liu, J. A. Zhang, D. Shen, Z. Zhang, and W. Yu, 2018: Tropical cyclone boundary layer rolls in synthetic aperture radar imagery. *J. Geophys. Res. Oceans*, **123**, 2981–2996, <https://doi.org/10.1029/2018JC013755>.
- Kain, J. S., 2004: The Kain–Fritsch convective parameterization: An update. *J. Appl. Meteor.*, **43**, 170–181, [https://doi.org/10.1175/1520-0450\(2004\)043<0170:TKCPAU>2.0.CO;2](https://doi.org/10.1175/1520-0450(2004)043<0170:TKCPAU>2.0.CO;2).
- Katsaros, K. B., P. W. Vachon, P. G. Black, P. P. Dodge, and E. W. Uhlhorn, 2000: Wind fields from SAR: Could they improve our understanding of storm dynamics? *Johns Hopkins APL Tech. Dig.*, **21**, 86–93, <https://doi.org/10.4095/219617>.
- , —, W. T. Liu, and P. G. Black, 2002: Microwave remote sensing of tropical cyclones from space. *J. Oceanogr.*, **58**, 137–151, <https://doi.org/10.1023/A:1015884903180>.
- Keptert, J., 2001: The dynamics of boundary layer jets within the tropical cyclone core. Part I: Linear theory. *J. Atmos. Sci.*, **58**, 2469–2484, [https://doi.org/10.1175/1520-0469\(2001\)058<2469:TDOBLJ>2.0.CO;2](https://doi.org/10.1175/1520-0469(2001)058<2469:TDOBLJ>2.0.CO;2).
- , and Y. Wang, 2001: The dynamics of boundary layer jets within the tropical cyclone core. Part II: Nonlinear enhancement. *J. Atmos. Sci.*, **58**, 2485–2501, [https://doi.org/10.1175/1520-0469\(2001\)058<2485:TDOBLJ>2.0.CO;2](https://doi.org/10.1175/1520-0469(2001)058<2485:TDOBLJ>2.0.CO;2).
- Kunin, P., D. Rostkier-Edelstein, and P. Alpert, 2019: High-resolution WRF simulations of the Mediterranean Sea breeze penetration into the Dead Sea valley: Sensitivity tests and optimal model configuration. *Geophysical Research Abstracts*, Vol. 21, Abstract 2060, <https://meetingorganizer.copernicus.org/EGU2019/EGU2019-2060.pdf>.
- LeMone, M. A., 1973: The structure and dynamics of horizontal roll vortices in the planetary boundary layer. *J. Atmos. Sci.*, **30**, 1077–1091, [https://doi.org/10.1175/1520-0469\(1973\)030<1077:TSADOH>2.0.CO;2](https://doi.org/10.1175/1520-0469(1973)030<1077:TSADOH>2.0.CO;2).
- Li, X., N. E. Davidson, Y. Duan, K. J. Tory, Z. Sun, and Q. Cai, 2020: Analysis of an ensemble of high-resolution WRF simulations for the rapid intensification of Super Typhoon Rammasun (2014). *Adv. Atmos. Sci.*, **37**, 187–210, <https://doi.org/10.1007/s00376-019-8274-z>.
- Lilly, D. K., 1966: On the instability of Ekman boundary flow. *J. Atmos. Sci.*, **23**, 481–494, [https://doi.org/10.1175/1520-0469\(1966\)023<0481:OTIOEB>2.0.CO;2](https://doi.org/10.1175/1520-0469(1966)023<0481:OTIOEB>2.0.CO;2).
- Lin, Y., and K. E. Mitchell, 2005: The NCEP stage II/IV hourly precipitation analyses: Development and applications. Preprints, *19th Conf. on Hydrology*, San Diego, CA, Amer. Meteor. Soc., 1.2, file://s1hcifs01/DEMProfiles/16352/Downloads/83847.pdf.
- Lorsolo, S., J. L. Schroeder, P. Dodge, and F. Marks Jr., 2008: An observational study of hurricane boundary layer small-scale coherent structures. *Mon. Wea. Rev.*, **136**, 2871–2893, <https://doi.org/10.1175/2008MWR2273.1>.
- Mlawer, E. J., S. J. Taubman, P. D. Brown, M. J. Iacono, and S. A. Clough, 1997: Radiative transfer for inhomogeneous atmospheres: RRTM, a validated correlated-k model for the longwave. *J. Geophys. Res.*, **102**, 16 663–16 682, <https://doi.org/10.1029/97JD00237>.
- Morrison, I., S. Businger, F. Marks, P. Dodge, and J. A. Businger, 2005: An observational case for the prevalence of roll vortices in the hurricane boundary layer. *J. Atmos. Sci.*, **62**, 2662–2673, <https://doi.org/10.1175/JAS3508.1>.
- Mourad, P. D., and B. A. Walter, 1996: Viewing a cold air outbreak using satellite-based synthetic aperture radar and Advanced Very High Resolution Radiometer imager. *J. Geophys. Res.*, **101**, 16 391–16 400, <https://doi.org/10.1029/96JC01123>.
- Nakanishi, M., and H. Niino, 2012: Large-eddy simulation of roll vortices in a hurricane boundary layer. *J. Atmos. Sci.*, **69**, 3558–3575, <https://doi.org/10.1175/JAS-D-11-0237.1>.
- Nolan, D. S., D. P. Stern, and J. A. Zhang, 2009: Evaluation of planetary boundary layer parameterizations in tropical cyclones by comparison of in situ observations and high-resolution simulations of Hurricane Isabel (2003). Part II: Inner-core boundary layer and eyewall structure. *Mon. Wea. Rev.*, **137**, 3675–3698, <https://doi.org/10.1175/2009MWR2786.1>.
- Skamarock, W. C., and Coauthors, 2008: A description of the Advanced Research WRF version 3. NCAR Tech. Note NCAR/TN-475+STR, 113 pp., <https://doi.org/10.5065/D68S4MVH>.
- Thompson, G., P. R. Field, R. M. Rasmussen, and W. D. Hall, 2008: Explicit forecasts of winter precipitation using an improved bulk microphysics scheme. Part II: Implementation of a new snow parameterization. *Mon. Wea. Rev.*, **136**, 5095–5115, <https://doi.org/10.1175/2008MWR2387.1>.
- Wang, S., and Q. Jiang, 2017: Impact of vertical wind shear on roll structure in idealized hurricane boundary layers. *Atmos. Chem. Phys.*, **17**, 3507–3524, <https://doi.org/10.5194/acp-17-3507-2017>.
- Weckwerth, T. M., J. W. Wilson, R. M. Wakimoto, and N. A. Crook, 1997: Horizontal convective rolls: Determining the environmental conditions supporting their existence and characteristics. *Mon. Wea. Rev.*, **125**, 505–526, [https://doi.org/10.1175/1520-0493\(1997\)125<0505:HCRDTE>2.0.CO;2](https://doi.org/10.1175/1520-0493(1997)125<0505:HCRDTE>2.0.CO;2).
- Wu, L., Q. Liu, and Y. Li, 2019: Tornado-scale vortices in the tropical cyclone boundary layer: Numerical simulation with the WRF–LES framework. *Atmos. Chem. Phys.*, **19**, 2477–2487, <https://doi.org/10.5194/acp-19-2477-2019>.
- Wurman, J., and J. Winslow, 1998: Intense sub-kilometer-scale boundary layer rolls observed in Hurricane Fran. *Science*, **280**, 555–557, <https://doi.org/10.1126/science.280.5363.555>.
- , and K. Kosiba, 2018: The role of small-scale vortices in enhancing surface winds and damage in Hurricane Harvey (2017). *Mon. Wea. Rev.*, **146**, 713–722, <https://doi.org/10.1175/MWR-D-17-0327.1>.
- Young, G. S., D. A. Kristovich, M. R. Hjelmfelt, and R. C. Foster, 2002: Supplement to rolls, streets, waves, and more. *Bull.*

- Amer. Meteor. Soc.*, **83**, 1001, <https://doi.org/10.1175/BAMS-83-7-Young>.
- Zhang, F., and Z. Pu, 2017: Effects of vertical eddy diffusivity parameterization on the evolution of landfalling hurricanes. *J. Atmos. Sci.*, **74**, 1879–1905, <https://doi.org/10.1175/JAS-D-16-0214.1>.
- , ———, and C. Wang, 2017: Effects of boundary layer vertical mixing on the evolution of hurricanes over land. *Mon. Wea. Rev.*, **145**, 2343–2361, <https://doi.org/10.1175/MWR-D-16-0421.1>.
- Zhang, J. A., K. B. Katsaros, P. G. Black, S. Lehner, J. R. French, and W. M. Drennan, 2008: Effects of roll vortices on turbulent fluxes in the hurricane boundary layer. *Bound.-Layer Meteor.*, **128**, 173–189, <https://doi.org/10.1007/s10546-008-9281-2>.
- , R. F. Rogers, D. S. Nolan, and F. D. Marks Jr., 2011: On the characteristic height scales of the hurricane boundary layer. *Mon. Wea. Rev.*, **139**, 2523–2535, <https://doi.org/10.1175/MWR-D-10-05017.1>.
- Zhu, P., 2008a: A multiple scale modeling system for coastal hurricane wind damage mitigation. *Nat. Hazards*, **47**, 577–591, <https://doi.org/10.1007/s11069-008-9240-8>.
- , 2008b: Simulation and parameterization of the turbulent transport in the hurricane boundary layer by large eddies. *J. Geophys. Res.*, **113**, D17104, <https://doi.org/10.1029/2007JD009643>.
- , Y. Wang, S. Chen, M. Curcic, and C. Gao, 2016: Impact of storm-induced cooling of sea surface temperature on large turbulent eddies and vertical turbulent transport in the atmospheric boundary layer of Hurricane Isaac. *J. Geophys. Res. Oceans*, **121**, 861–876, <https://doi.org/10.1002/2015JC011320>.